(1)

ARMY RESEARCH LABORATORY

SALTATION AND SUSPENSION OF SEDIMENT BY TURBULENT WIND

PHASE I FINAL REPORT

Paul A. Hwang
Quest Integrated, Inc.
21414-68th Avenue South
Kent, Washington 98032

Under Contract DAAL06-92-C-0010
Contract Monitor Frank V. Hansen

ARL-CR-6 *December 1992*

Approved for public release; distribution unlimited.

NOTICES

Disclaimers

The findings in this report are not to be construed as an official Department of the Army position, unless so designated by other authorized documents.

The citation of trade names and names of manufacturers in this report is not to be construed as official Government indorsement or approval of commercial products or services referenced herein.

Destruction Notice

When this document is no longer needed, destroy it by any method that will prevent disclosure of its contents or reconstruction of the document.

REPORT DOCUMENTATION PAGE

Form Approved
OMB No. 0704-0188

1. AGENCY USE ONLY (Leave blank)	2. REPORT DATE	3. REPORT TYPE AND DATES COVERED
	December 1992	Final

4. TITLE AND SUBTITLE
SALTATION AND SUSPENSION OF SEDIMENT BY TURBULENT WIND PHASE I FINAL REPORT

5. FUNDING NUMBERS
62784/AH71 (6.2)

6. AUTHOR(S)
Paul A. Hwang

7. PERFORMING ORGANIZATION NAME(S) AND ADDRESS(ES)
Quest Integrated, Inc.
21414-68th Avenue South
Kent, Washington 98032

8. PERFORMING ORGANIZATION REPORT NUMBER

9. SPONSORING / MONITORING AGENCY NAME(S) AND ADDRESS(ES)
U.S. Army Research Laboratory
Battlefield Environment Directorate
White Sands Missile Range, NM 88002-5501

10. SPONSORING / MONITORING AGENCY REPORT NUMBER
ARL-CR-6

11. SUPPLEMENTARY NOTES
Frank V. Hansen (Contract Monitor)

12a. DISTRIBUTION / AVAILABILITY STATEMENT
Approved for public release; distribution unlimited.

12b. DISTRIBUTION CODE

13. ABSTRACT *(Maximum 200 words)*

Particles in the air absorb and scatter electromagnetic waves, causing transmission loss and image obscuration. The patterns of scattering and extinction are functions of wavelength, particle size, and particle number. In order to calculate the transmittance and extinction of multispectral target acquisition sensors, the number density and size distribution of particles along the target path need to be provided. Because the airborne particles are derived mainly from terrestrial sources, the distribution of airborne particles is critically controlled by the sediment transport processes. This study takes advantage of the extensive results and experience from sediment transport research in an attempt to develop an efficient algorithm of deriving the information of airborne particle distribution as a function of various environmental parameters.

14. SUBJECT TERMS	15. NUMBER OF PAGES
Concentration, eolian, mass flux, saltation, sediment transport, size distribution, spherical coordinates, suspension	37
	16. PRICE CODE

17. SECURITY CLASSIFICATION OF REPORT	18. SECURITY CLASSIFICATION OF THIS PAGE	19. SECURITY CLASSIFICATION OF ABSTRACT	20. LIMITATION OF ABSTRACT
Unclassified	Unclassified	Unclassified	SAR

TABLE OF CONTENTS

LIST OF FIGURES AND TABLES

LIST OF SYMBOLS

a	Particle diameter.
a_0	Reference diameter (0.025 cm).
a_m	Median diameter.
c	Sediment concentration.
C	Mean concentration.
C_a	Reference concentration at elevation z_a.
c'	Fluctuation component of concentration.
D	Elevation of target acquisition system.
f	Function representing the vertical decay of airborne particles, $f(z) = (z/z_r)^{-m}$.
F_D	Drag force on a particle.
F_G	Gravitational force on a particle.
g	Gravitational acceleration.
k	Dynamic roughness (immobile surface).
k'	Dynamic roughness of a movable surface.
l	Saltation length; also the exponent of the size-shape function in the large particle region.
m	Mass of sediment particles; also the exponent of vertical distribution function, see f.
M_D	Moment about the resting point of a particle due to fluid drag force.
M_G	Moment about the resting point of a particle due to gravitational force.
n	Number density of size distribution [$n(a, z)$]; also size-shape function [$n(a)$].
N	Integrated number of airborne particles within the propagation path of a target acquisition system; also integrated number of particles over the size range.
p	Probability distribution function of source sediment.
q	Sediment transport rate.
r	Exponent of the particle size-shape function.
Re	Reynolds number.
s	The exponent of the size-shape function in the small particle region.
t	Time coordinate.
u	Velocity.
u_1	Horizontal component of liftoff velocity.
u_2	Horizontal component of impact velocity.
u_*	Wind friction velocity, related to wind stress by $u_*=(\tau/\rho)^{1/2}$.
U	Wind velocity.
U_p	Particle convective velocity.
w_1	Vertical component of liftoff velocity.
w_f	Particle fall velocity.
(x, y, z)	Cartesian coordinate system: x is along prevailing wind, y is cross-wind, and z is positive upward.
z_0	Dynamic roughness of a surface.
z_1	Lower limit of saltation layer, assumed to be one diameter high.
z_2	Upper limit of saltation layer, that is, saltation height of particle.
z_a	Reference elevation of the concentration profile.
z_r	Reference elevation in the expression of the vertical distribution function, $f(z)$.

LIST OF SYMBOLS (Cont.)

α	Angle of repose.
(ρ, ϕ, θ)	Spherical coordinate system: ρ is range, ϕ is zenith angle, and θ is azimuthal angle.
κ	von Karman's constant (=0.4).
ν	Fluid viscosity.
ν_x, ν_y, ν_z	Turbulent viscosity in the x-, y-, and z-directions.
ρ	Density of fluid; also range in the spherical coordinates.
ρ_s	Density of solid particle.
τ	Surface wind stress.

1. INTRODUCTION

Airborne particles scatter and absorb electromagnetic (EM) waves and affect the performance of target acquisition systems. The extinction due to particles depends primarily on the ratio of the particle size and the EM wavelength. Because the wavelengths used in the Army target acquisition systems and other remote sensors range from visible to infrared optical wave bands and millimeter radar waves to low-frequency acoustic waves, the particle sizes that need to be monitored range from those of gas and aerosols to coarse sand. This research project seeks to develop an accurate model for predicting the number concentration and size distribution of airborne sediment particles (including sand and dust) from saltation and suspension caused by turbulent wind.

The transport problems have been investigated by researchers in many different fields, including atmospheric science, geological science, agricultural engineering, chemical engineering, mechanical engineering, ocean engineering, and civil engineering. The amount of research results and literature references is extensive and diversified. Much of the work has been reviewed by Bagnold (1941), Raudkivi (1976), Yalin (1977), Clift et al. (1978), Hwang (1982), Sleath (1984), Greeley and Iversen (1985), Anderson (1986), Werner (1987, 1990), and Dyer and Soulsby (1988), among others. The material presented in this section represents merely a small drop in a very big bucket.

In general, there are three major modes of sediment transport: creeping, saltation, and suspension. For wind (eolian) transport of sand on land, saltation is of special importance because it dominates a rather thick layer (of the order of 1 meter, Bagnold, 1941) of the lower boundary. Suspension is important in the transport of fine dust and aerosols, which can be airborne for a long period of time (of the order of days or weeks, Toba, 1965). Creeping is confined in the immediate vicinity of the ground and contributes to a rather small fraction of the total transport (Bagnold, 1941; Nickling, 1978). From careful observations, Bagnold (p. 10, 1941) offered the following description of saltation and suspension in the open field:

> "A popular misconception exists regarding sand storms, due to a failure to distinguish sand from dust. When, in any arid country, after a spell of calm weather, a strong wind begins to blow from a new direction, the air becomes charged with a mist of small particles. Where the surface is alluvial, with little or no sand on it, such as in Iraq or the country round Khartoum, the dust rises in dense clouds to a height of several thousand feet and the sun is obscured for a long period. This is obviously a dust storm, though it is often wrongly designated by the possibly more thrilling and cleanly term 'sand storm'. Owing to their feeble terminal velocity of fall the very small dust particles are raised and kept aloft by the upward currents of the wind's internal movements . . .
>
> On the other hand, in an erosion desert, the only free dust consists of those fine rock particles which have been loosened by weathering since the last wind blew, and have therefore not been carried away. In such country the wind produces for the first hour or so a mist consisting of both dust and sand. Later, although the wind may have shown no signs of slackening, the mist disappears. But the sand still continues to drive across country as a thick, low-flying cloud with a clearly marked upper surface. The air above the sand cloud becomes clear, the sun shines again, and people's heads and shoulders can often be seen projecting above the cloud as from the water of a swimming-bath. Where the ground is composed of coarse grains, pebbles, or large stones, the top of the cloud may be 2 metres above it, but is usually less. Where the surface consists of fine sand, such as that of a dune, the height of the sand cloud is noticeably lower."

The description above clearly indicates the possible serious effects of eolian processes in the operation of a target acquisition system and other remote sensing devices. It is noted that the physical mechanisms governing the aerosol transport process are very complicated, as reflected from the fact that the sources of aerosol particles can be from many thousand miles away; there is no reliable model to describe the aerosol motion; and our understanding of aerosol distributions relies on experimental measurements. Results on the size distribution of aerosols have been generally classified into major categories such as Urban, Rural, Remote continental, Desert dust storm, Polar, Stratosphere, Sea salt and Background (e.g., Junge, 1972; Jaenicke, 1988). For larger particles, including sand grains and dust particles, the distribution is more localized and amenable (in a relative sense) to mathematical treatment. The capability to establish the transport rate or concentration profiles as functions of wind and particle parameters underscores the significant advance of our understanding of the large particle dynamics (although admittedly still far away from perfect or even satisfactory).

With the advance of digital computers, many numerical models have been developed. Mechanisms such as sediment-wind interaction and the random nature of parameters, including particle inception by wind force, variability of ejection angles, impact angles, number of particles mobilized by impact, and particle trajectories subjected to drag, lift, and spinning effects, can be incorporated (e.g., Owen, 1964; White and Schulz, 1977; Anderson, 1986; Anderson and Hallet, 1986; Ungar and Haff, 1987; Anderson and Haff, 1988, 1990; Haff and Anderson, 1989; Werner, 1990). These models enhance our understanding of the physics of sediment transport considerably. It is noted that such numerical models are computationally intensive and may take hours or even days to complete a "run" of relatively simple scenario (Haff, personal communication, 1991); thus, the applicability to field use remains limited.

Although practical application using results from modern numerical simulations on the physics of sediment transport appears to be remote, there are some robust, time-tested relationships derived from sediment research that deserve a closer examination. One of the most significant developments is the establishment of sediment transport rate equations, formulated to predict the flux of sediment as a function of wind and particle properties. The development of these formulas was based on the consideration of momentum balance between airborne sediment and wind motion, as well as data fitting to account for physical mechanisms that were not easily formulated mathematically (Bagnold, 1941). Since Bagnold's milestone work, numerous new equations have been introduced, but time and again the fundamental physical mechanism described by Bagnold was found to be rather accurate.

The transport rate equation, however, provides the total sediment flux only and offers very poor size resolution. As mentioned earlier, for remote sensing applications, a good understanding of the size distribution of airborne particles is critical because the properties of absorption, scattering, and extinction are wavelength- and particle-size-dependent (e.g., Mie, 1908; Rayleigh, 1945; Sommerfeld, 1950; van de Hulst, 1981). In order to apply the results of sediment transport research to target acquisition applications, we need to develop a sequence of mathematical manipulations to bring out the inherent information of the size distribution function of airborne particles. This is done by introducing an equivalent concentration to represent the saltation particles. By equating the transport rate with the rate of sediment flux (the product of concentration and convective velocity) over the saltation layer, it is possible to recover the information of the size distribution. With the size distribution known, the number of airborne particles within the path of a target acquisition system can be calculated.

For smaller particles that may suspend in the air once lifted from the ground, the dominant process is turbulent diffusion. With proper assumptions of eddy diffusivity, the resulting concentration profiles decay with distance from the bottom boundary following either a power law, an exponential distribution, or some combined form of both (e.g., Hwang, 1982). The suspension and saltation processes are closely related. In particular, the impact of saltation particles causes the dislodging of small dust particles to start the

suspension process, and the saltation layer controls the boundary condition of the suspension layer. The number density and size distribution of the saltation layer determine the absolute concentration of the much thicker suspension layer. Coupling of these two layers is important in deriving the total density of particles under any given configuration of a target acquisition system.

In order to interface with the operations of target acquisition systems, a procedure for coordinate conversion from Cartesian coordinates to spherical coordinates is developed. Computational examples show that the integrated number of particles within a pencil beam of a remote sensor increases significantly as the incident angle increases; a few orders of magnitude increase from 10° to 80° is common for a typical vertical stratification of airborne particle distribution.

This report documents a Phase I study to evaluate and develop models of the saltation and suspension of sediment by turbulent transport. In Section 2, a brief discussion is presented of the theoretical background of saltation, suspension, the flux formulation to retrieve the size distribution information, and the mathematical aspect of coordinate transformation from Cartesian to spherical coordinates. In Section 3, a comparison and evaluation is given of a small group of sediment transport rate equations. The parameterization scheme to facilitate numerical evaluation of number density from the flux formulation is given in Section 4. Results and discussions of sensitivity tests performed to investigate and rank the importance of numerous parameters are given in Sections 5 and 6, respectively, and recommendations for further research are presented in Section 7.

2. THEORETICAL BACKGROUND

Two modes of sediment transport are of special interest in the study of airborne particle distribution: suspension and saltation. The former governs the dispersion of smaller dust particles into the air, and the latter governs the ejection of larger sand grains from the surface. The impact of sand grains is an important mechanism for dislodging the smaller dust particles that are either shadowed by larger grains or present in the source material as aggregates.

2.1 Saltation

One of the most significant relationships derived from sediment transport research is the establishment of the transport rate as a function of the wind friction velocity or wind speed. Because the contribution of different size classes to the total sediment transport is proportional to the volumes of the size classes, the transport rate is dominated by the larger particles, which move in the air in saltation. For example, Bagnold (1941) reported that, for regular desert sand, the saltation load is 80% of the total sediment flux. To establish a relationship between the transport rate and the turbulent wind condition, Bagnold (1941) considered the momentum balance of airborne particles. Starting with a saltating particle of mass m that rises from the surface with a horizontal velocity u_1 and strikes on the surface again after traveling a distance l with a horizontal velocity u_2, and assuming that all of the horizontal momentum was lost after impact, the averaged momentum extracted from the air per unit length is therefore $m(u_2-u_1)/l$. Extending the concept of one grain to the mass flux of sand q, the rate of momentum loss of air becomes $q(u_2-u_1)/l$. This momentum loss results in a resisting force τ on the surface, if $u_1 << u_2$, and the following expression is established:

$$q\frac{u_2}{l} = \tau = \rho u_*^2 \tag{1}$$

where ρ is the density of air and u_* is the wind friction velocity. From grain path analysis, Bagnold further found that over a wide range of values, $u_2/l = g/w_1$, where w_1 is the initial vertical velocity of rise of the grain at the beginning of its path and g is the gravitational acceleration. The sediment flux becomes

$$q = \frac{\rho}{g} u_*^2 w_1 \tag{2}$$

Assuming that w_1 is proportional to u_*, based on the argument that the grains are exposed to the air stream at all heights and that their mean velocity of impact is likely to be controlled by u_* which defined the wind speed distribution, Bagnold reached the conclusion that the rate of sediment flux q is proportional to the cubic power of the wind friction velocity:

$$q = B\left(\frac{a}{a_0}\right)^{1/2} \frac{\rho}{g} u_*^3 \tag{3}$$

where a is the representative grain diameter of the source sediment, a_0 = 0.025 cm is a reference sand size and B is an empirical coefficient determined to be 1.5 for a nearly uniform sand, 1.8 for naturally graded sands, such as those found on sand dunes, and 2.8 for a sand with a very wide range of grain sizes. A great number of newer equations have been suggested over the past few decades (e.g., see Greeley and Iversen, 1985; Sarre, 1987), but the fundamental physics of momentum balance between sand flow and wind motion has not changed, and nearly all of the formulas maintain the cubic power law relationship (either directly with wind friction velocity or the velocity scale representing the excess wind stress, which is the difference of wind stress and particle threshold stress).

2.2 Suspension

Particle suspension is governed by turbulent diffusion in the fluid. This is generally formulated as the balance of turbulence agitation with flow convection and gravitational settling. Efforts to study the suspension problem have been performed by many scientists in various fields, such as atmospheric science, hydraulics, oceanography, coastal engineering, chemical engineering, agriculture, and environmental science. The process can be expressed as (e.g., Yalin, 1977; Hwang, 1982; Anderson, 1986)

$$\frac{\partial c}{\partial t} + \nabla \bullet (\mathbf{u}_p c) = \nabla \bullet (\nu \nabla c) \tag{4}$$

where c is the (volumetric) concentration of the suspended particles, $\mathbf{u}_p$ the convective velocity vector of the particles, ν the fluid (air) viscosity and t the time. It is common to express the variables c and $\mathbf{u}_p$ in two components: the mean and the fluctuation (due to the turbulent nature of the process); that is, $c = C + c'$ and $\mathbf{u}_p = \mathbf{U}_p + \mathbf{u}_p'$. The equation governing the mean concentration becomes

$$\frac{\partial C}{\partial t} + \nabla \bullet \left(\langle C \mathbf{U}_p \rangle + \langle c' \mathbf{u}_p' \rangle \right) = \nabla \bullet (\nu \nabla C) \tag{5}$$

where the angle brackets represent the mean value (ensemble or temporal average) of the bracketed property. A turbulent diffusivity coefficient is usually introduced to represent the diffusion term of the turbulent "flux":

$$\nabla \bullet \langle c' \mathbf{u}_p' \rangle = \nu_x \frac{\partial C}{\partial t} + \nu_y \frac{\partial C}{\partial t} + \nu_z \frac{\partial C}{\partial t} \tag{6}$$

where ν_x, ν_y, and ν_z are the turbulent diffusivity in the x-, y-, and z-directions. The solution of Eq. (5) depends very much on the turbulence properties of the flow field. Due to our limited understanding of flow turbulence, closed-form solutions are available only for a few simplified conditions. For example, under the assumptions of temporal steadiness and horizontal homogeneity, also neglecting the term of molecular diffusion in comparison with the turbulent diffusion terms, the resulting equation becomes

$$C w_f = -\nu_z \frac{\partial C}{\partial z} \tag{7}$$

where w_f is the fall velocity of the particle. The solution of Eq (7) is

$$C(z) = C_a \exp\left[-\int_{z_a}^{z} \frac{w_f}{\nu_z} dz \right] \tag{8}$$

in which C_a is the reference concentration at elevation z_a. Depending on the definition of the turbulent diffusivity, the distribution follows either an exponential (for ν_z constant) or power-law (for ν_z proportional to z) decay with distance from the boundary. Other more complicated definitions of ν_z would lead to more complicated vertical profiles of suspension. The rapid decay from the boundary remains the common feature and stresses the importance of including the vertical variation of dust and aerosol distribution when the results are to be applied close to the boundary.

When the bottom material is not composed of uniform-size particles, the size distribution of the source material needs to be taken into consideration. If the interaction between different size classes is negligible, linear superposition can be applied and the resulting total concentration is

$$C'(z) = \int_0^\infty p(a) C(a,z) da \tag{9}$$

where $p(a)$ is the size distribution of bottom material and $C(a, z)$ is the suspension of an individual size class, which takes the fonn of Eq. (8) with the fall velocity and turbulent diffusivity properly determined for each size class.

2.3 Sediment Flux and Size Distribution

From empirical observations, it is generally found that the ratio of saltation and suspension transport is approximately constant. Bagnold (1941) found that the ratio is 4:1 based on laboratory measurements using sand ranging in size from 0.1 to 1.0 mm. Nickling (1983) conducted field measurements on the Slims River Valley, Yukon Territory, where the mean sediment size is considerably finer (0.06 to 0.12 mm) and the fraction of suspension increases to as much as 69% of the total transport. Regardless of the exact proportionality of saltation versus suspension, the sediment transport rate can be expressed in terms of the airborne sediment concentration, $C(a, z)$, here representing the sum of suspension and saltation. The volume concentration, $C(a, z)$, is further related to the size distribution of the suspension, $n(a, z)$, by

$$C(a,z) = n(a,z)\frac{4\pi a^3}{3} \tag{10}$$

By definition, the transport rate can be written as the vertical integration of the product of sediment concentration and convective velocity, i.e.,

$$q = \iint n(a,z)\ \frac{4\pi a^3}{3} U_p(a;z)\, da\, dz \tag{11}$$

Combining Eqs. (3) and (11), it is immediately obvious that the size distribution as a function of wind condition and surface material property can be obtained from the sediment transport formula:

$$\int_{z_1}^{z_2}\int_{a_1}^{a_2} n(a,z)\ \frac{4\pi a^3}{3} U_p(a,z)\, da\, dz = B\left(\frac{a_m}{a_0}\right)^{1/2}\frac{\rho}{g}u_*^3 \tag{12}$$

where the integration limits are explicitly expressed as $[a_1, a_2]$ and $[z_1, z_2]$, respectively. Equation (12) contains many unknowns including the size distribution function $n(a, z)$, the convective velocity U_p, and the four variables defining the integration limits. Our primary tasks are to provide additional relationships based on theoretical, numerical, and experimental results so that enough equations can be formulated to solve for the size distribution function. For example, the integration limits $[a_1, a_2]$ represent the range of particle sizes that can be mobilized under a given wind condition, which can be derived from our knowledge of the threshold criterion of particle motion; and the factor z_2 defines the upper limit of integration, which is properly interpreted as the saltation height. More discussion of the parameterization is given in Section 4.

2.4 Spherical Coordinates Transformation

The sediment concentration or mass flux formulas are generally developed in the rectangular coordinate system. To predict the concentration of airborne sand and dust along the path between observer and target, it is more useful to express these terms in spherical coordinates. Fig. 1 shows the two coordinate systems from which the following relationships can be established:

$$x = \rho \sin\phi \cos\theta \tag{13}$$

$$y = \rho \sin\phi \sin\theta \tag{14}$$

$$z = \rho \cos\phi + D \tag{15}$$

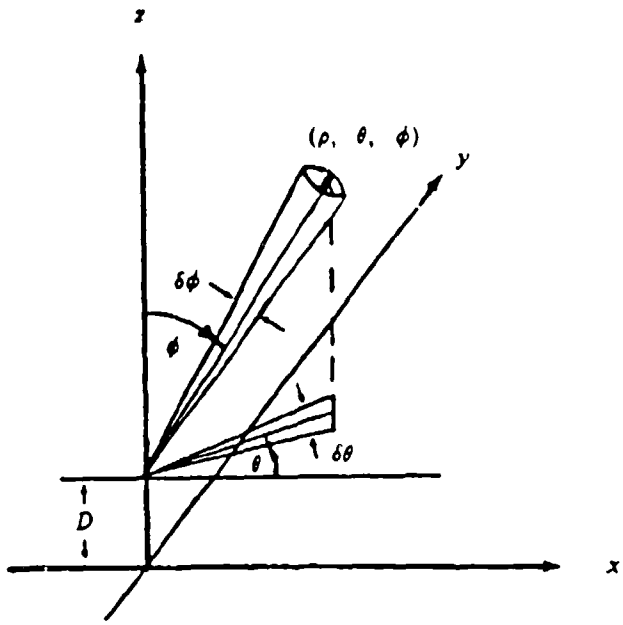

Figure 1. Sketch depicting the wave path of a target acquisition system in rectangular Cartesian coordinate system and spherical coordinate system.

(Note the symbols used here follow the mathematical convention with ϕ as the zenith angle and θ as the azimuthal angle. In radar applications, θ and ϕ are usually reversed, that is, θ is the incident or zenith angle and ϕ the azimuthal angle). The vertical offset D is the elevation of the target acquisition system. The integration region of interest is the path cone shown in the figure. Because the extinction parameter of the target acquisition system is sensitive to the instrument wavelength and particle size, the desired quantity from the saltation algorithm is the concentration of particles of a given size, that is, the size distribution $n(a; \rho, \theta, \phi)$ at different ranges and azimuth and zenith angles. With the size distribution given in the rectangular coordinates, the transformation to spherical coordinates, and the integration to obtain the integrated size distribution within the path cone can be obtained using Eqs. (13) through (15). As discussed earlier, we have assumed horizontal homogeneity in the airborne particle distribution; thus, the only function involved in the coordinate transformation is the vertical distribution function. Following the notation to be used in Section 4, we can write $n(a; \rho, \theta, \phi) = n(a, z) = Kn(a)f(a; z)$, where $f(a; z) = f(a; \rho\cos\phi)$ is the vertical distribution function. The number of particles integrated over the path cone is therefore proportional to

$$F(a) = \iiint_{vol} f(a;z)\, dx\, dy\, dz = \iiint_{vol} f(a;\rho\cos\phi)\, \rho^2 \sin\phi\, d\rho\, d\phi\, d\theta \tag{16}$$

where $\rho^2\sin\phi$ is the Jacobian of the coordinate transformation, $F(a)$ is the integrated function, and *vol* denotes the volume of the air space within the wave path, as defined in Fig. 1:

$$vol = \left(0 < \rho < R,\ -\frac{\delta\theta}{2} < \theta < \frac{\delta\theta}{2},\ \frac{\phi_0 - \delta\theta}{2} < \phi < \frac{\phi_0 + \delta\theta}{2}\right) \tag{17}$$

Using the solid angle expression as in remote sensing applications, Eq. (16) can be written as

$$F(a) = \iiint_{vol} f(a; \rho\cos\phi)\, \rho^2\, d\Omega \tag{18}$$

where $d\Omega = \sin\phi\, d\phi\, d\theta$ is the element of the solid angle. The functional dependence of $f(\phi)$ suggests that the inclusion of airborne particles in the remote sensing computation is equivalent to introducing a modification of the antenna pattern (e.g., Kerr, 1951; Stutzman and Thiele, 1981). The transformation of the

cross-sectional area and volume concentration of particles in the path cone can be derived in a similar fashion as that of the number density, Eq. (16).

For a smooth function f such as generally encountered in the vertical distribution of airborne particles, the integral can be carried out and a closed-form solution is available. For example, if the vertical distribution of airborne particles follows a power-law decay form, $f(z) = z^{-m}$, the integrated number of particles within a pencil beam of a target acquisition system is shown in Fig. 2 as a function of the incident angle. In this figure, the computed number is normalized such that when the particle distribution is uniform ($m = 0$), the integrated number is 1. As clearly illustrated in the figure, at a low grazing angle (high incident angle), the encountered number of airborne particles can increase drastically, more than 1000-fold between 10° and 85° for $m = 2.9$. This large increase of particle concentration at the grazing angle can significantly affect the performance of target acquisition systems in near-ground-level applications.

2.5 Research Tasks

Four research tasks were identified for the Phase I effort:

- Task 1. Evaluation and selection of sediment transport formulas.
- Task 2. Derivation of size distribution from sediment flux formulation.
- Task 3. Establishment of parameterization scheme to facilitate numerical computation.
- Task 4 Performance of sensitivity tests and evaluation of the feasibility of the proposed concept to derive the size distribution function from sediment transport rate equations.

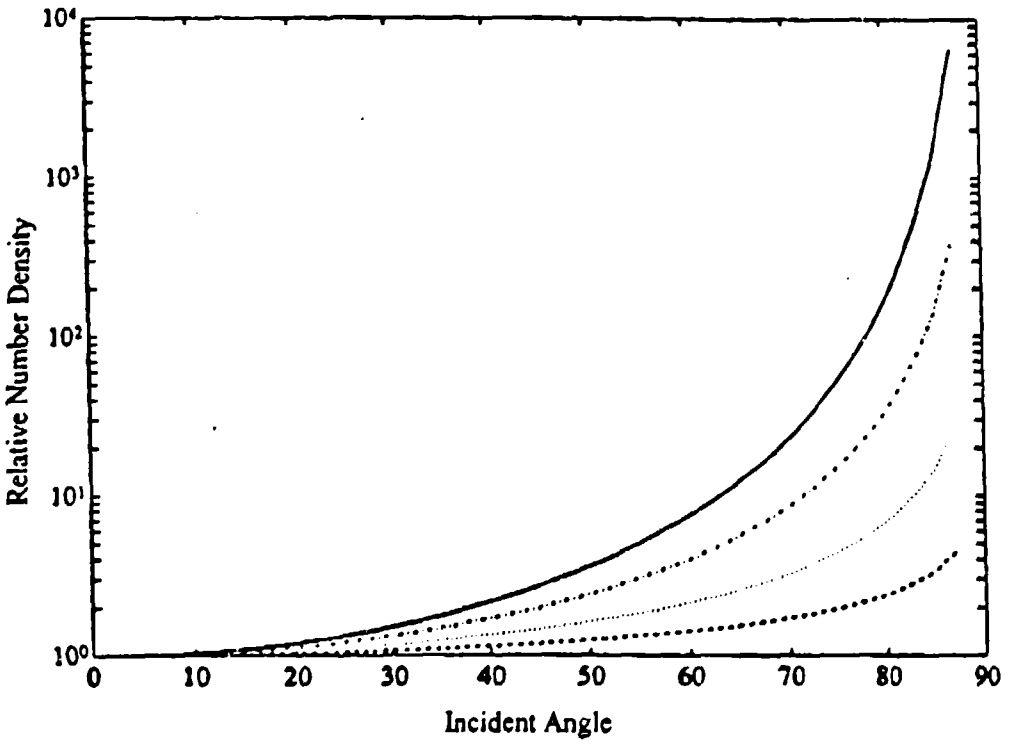

Figure 2. The effect of vertical distribution of airborne particles on variation of the integrated particle concentration within the pencil beam of a target acquisition system plotted as a function of incident angle. The vertical decay function $f(z)$ is assumed a power-law of the form z^{-m}. The number density for a uniform particle distribution (m=0) is used as the normalization factor. The normalized curves for m=0, 0.5, 1.1, 2, and 2.9 are shown.

3. COMPARISON OF SEDIMENT TRANSPORT RATE EQUATIONS

Seven sediment transport rate formulas [Eqs. (19) to (25) given in Table 1] are compared to evaluate the statistical difference among these equations. The common feature of these equations is the cubic-power wind dependence, either in terms of the wind friction velocity, u_*, or the wind speed at a given reference level, U_{100} (taken as 1 meter above the ground in this report). The more recent equations usually incorporate the threshold friction velocity in the formulation to emphasize that transport occurs only when the surface stress exceeds the resistance of grains to wind forcing. Formulas of Bagnold (1941) and Zingg (1952) do not contain u_{*t}, although the corresponding expressions using wind speed U have a threshold wind speed factored in Bagnold's case (p. 69, Bagnold, 1941). These equations are understood to be applied for $u_*>u_{*t}$. In this report, numerical computation based on the seven transport rate equations is performed for wind speeds ranging from 2 to 40 m/s and characteristic sediment diameters from 0.005 to 0.05 cm (50 to 500 μm). The results are presented in this section.

Table 1. Selected sediment transport rate equations evaluated in this study.

BA1 Bagnold (1941)	$q = 1.8\left(\frac{a}{a_0}\right)^{0.5}\frac{\rho}{g}u_*^3$	(19)
KA Kawamura (1951)	$q = 2.78\left(1+\left(\frac{u_{*t}}{u_*}\right)^2\right)\left(1-\frac{u_{*t}}{u_*}\right)\frac{\rho}{g}u_*^3$	(20)
L&L Lettau and Lettau (1978)	$q = 2.85\left(1-\frac{u_{*t}}{u_*}\right)\frac{\rho}{g}u_*^3$	(21)
IS Iversen et al. (1976); Schmidt (1982)	$q = 0.4\frac{w_f}{u_{*t}}\left(1-\frac{u_{*t}}{u_*}\right)\frac{\rho}{g}u_*^3$	(22)
OW Owen (1964)	$q = \left(0.25+0.33\frac{w_f}{u_*}\right)\left(1-\left(\frac{u_{*t}}{u_*}\right)^2\right)\frac{\rho}{g}u_*^3$	(23)
ZI Zingg (1952)	$q = 0.83\left(\frac{a}{a_0}\right)^{0.75}\frac{\rho}{g}u_*^3$	(24)
WH White (1979)	$q = 2.61\left(1+\frac{u_{*t}}{u_*}\right)^2\left(1-\frac{u_{*t}}{u_*}\right)\frac{\rho}{g}u_*^3$	(25)

3.1 Fundamental Parameters

Most of the transport rate equations are expressed in terms of the wind friction velocity, u_*, and the sediment diameter, a. The latter is one of the most important parameters of the bottom material. If the material is uniform (monodisperse), the definition of sediment size is straightforward. For mixed materials (polydisperse), the median size is usually used. Two other parameters that are also included in some of the transport rate equations are the threshold velocity, u_{*t}, and the particle settling velocity, w_f. The functional expressions of u_*, u_{*t}, and w_f are discussed in the following.

Wind Friction Velocity

The wind friction velocity is a measure of the wind stress applied on the sediment. If the bottom material is not moving, u_* and $U(z)$ are connected by the well-established logarithmic distribution (Bagnold, 1941; Schlichting, 1968)

$$U(z) = 5.75u_* \log\frac{z}{k} \tag{26}$$

where k is a length scale characterizing the surface roughness. For a flat surface covered with uniform sand, $k = a/30$. The wind friction velocity can be calculated from the reference wind velocity at 1 meter, U_{100}, by

$$u_* = \frac{U_{100}}{5.75\log\frac{(30)(100)}{a}} = \frac{U_{100}}{19.99 - 5.75\log a} \tag{27}$$

The vertical distribution of wind is modified by sand motion, as investigated in detail by Bagnold (1941). The resulting velocity profile is given as

$$U(z) = 5.75u_* \log\frac{z}{k'} + U_t \tag{28}$$

where the modified roughness, k', and threshold velocity, U_t, are functions of particle size. The following formulas (in cgs units) are adopted following the laboratory results of Zingg (1952; see also Horikawa, 1978; Horikawa et al., 1986):

$$k' = 10a \tag{29}$$

$$U_t = 8940a \tag{30}$$

The wind friction velocity on a movable boundary becomes

$$u_* = \frac{U_{100} - 8940a}{5.75\log\frac{100}{10a}} = \frac{U_{100} - 8940a}{5.75(1 - \log a)} \tag{31}$$

Again, the wind velocity at 1 meter is used as a reference. The wind friction velocity with a moving sediment bottom is considerably larger than that on a fixed rough boundary. Fig. 3 displays the computed results of Eqs. (27) and (31) for sediment size a=0.005, 0.01, ..., 0.05 cm. The friction velocity on moving sand (dotted curves) is nearly twice the magnitude of the fixed boundary results (solid curves) at higher wind velocities (U_{100}>10 m/s).

Bagnold also conducted field measurements on natural sand dunes and found that for *standard* sand dunes, k' = 1 cm and U_t = 4 m/s. With these values, the wind friction velocity would be

$$u_* = 0.087U_{100} - 34.7 \tag{32}$$

The calculated results using Eq. (32) are shown as x's in Fig. 3 also. It appears that Eq.(31) derived from laboratory results may underestimate the friction velocity; however, lacking a more comprehensive data set from field measurements, it is used in the following evaluation of various sediment transport equations.

Threshold Friction Velocity

As wind blows on a sandy surface, it exerts drag on sand grains. Due to gravitational stabilization, the sand grain resists the drag until wind exceeds some critical velocity (the threshold velocity) to set the sand particle in motion. The threshold velocity can be calculated by considering the balance of moments due to

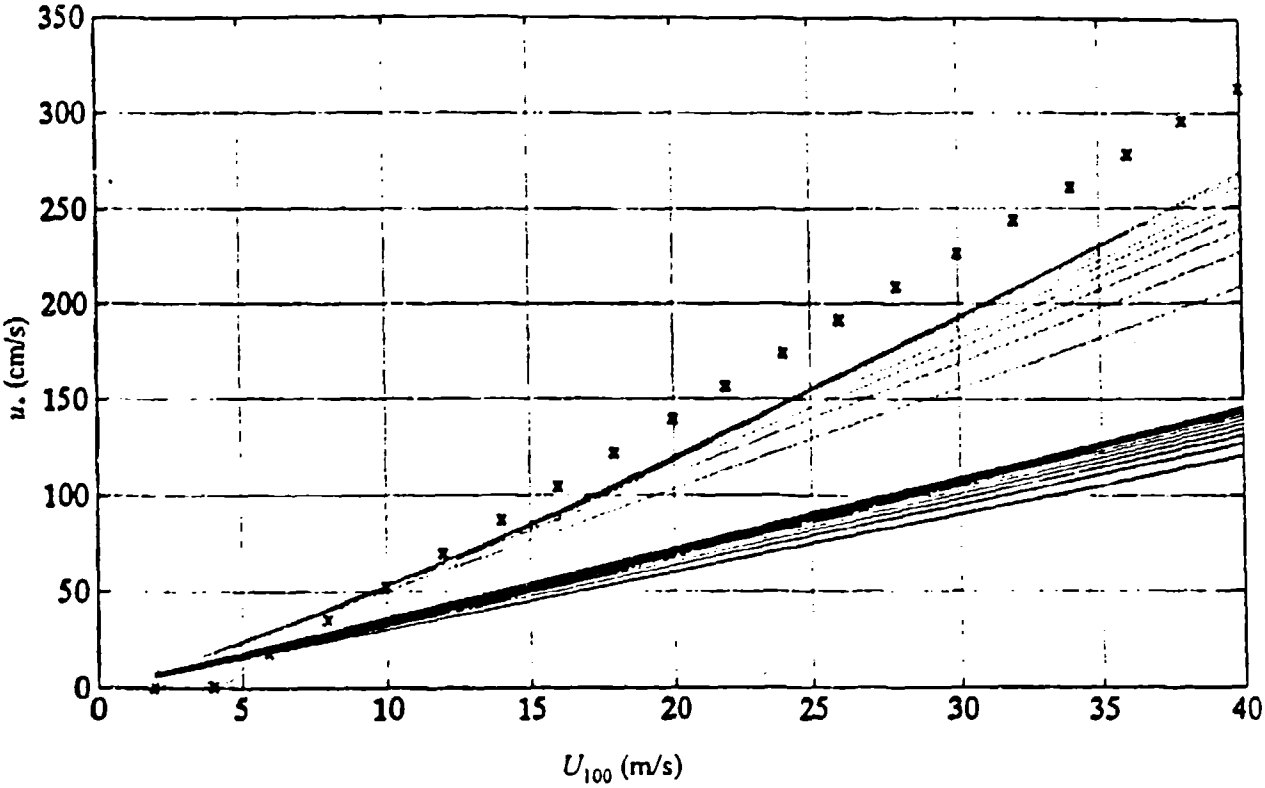

Figure 3. Wind friction velocity as a function of wind velocity at 1-meter elevation. Solid curves: rough turbulent boundary layer with fixed roughness elements (uniform sand of diameter from 0.005, 0.01, ..., 0.05 cm); u_* increases with increasing a for the same U_{100}. Dotted curves: movable boundary layer with uniform sand of the same diameter range as previous case. x: results corresponding to the field observations on *standard* sand dunes by Bagnold (1941).

the two competing forces, the wind drag, F_D, and the gravitational force, F_G (Bagnold, 1941). With reference to Fig. 4a, the two forces can be expressed as

$$F_G = \frac{\pi a^3}{6}(\rho - \rho_s)g \tag{33}$$

$$F_D = \frac{1}{2}\rho C_D U^2 \frac{\pi a^2}{4} A' \tag{34}$$

where A' is a factor representing the fraction of the particle cross-sectional area exposed to the flow, and C_D is the drag coefficient. Alternatively, $u_*^2 = C_D U^2$ can be substituted into Eq. (34) and the drag force expressed in terms of the friction velocity. The corresponding moments about the resting point of the grain from the two force components are

$$M_G = \frac{\pi a^3}{6}(\rho - \rho_s)g \cdot \frac{a}{2}\sin\alpha \tag{35}$$

$$M_D = \frac{1}{2}\rho u_*^2 \frac{\pi a^2}{4} A' \cdot \frac{a}{2}\cos\alpha \tag{36}$$

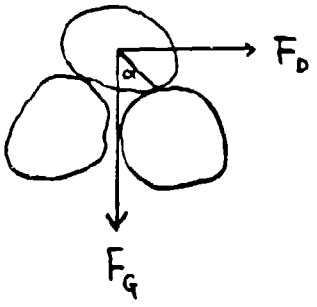

(a)

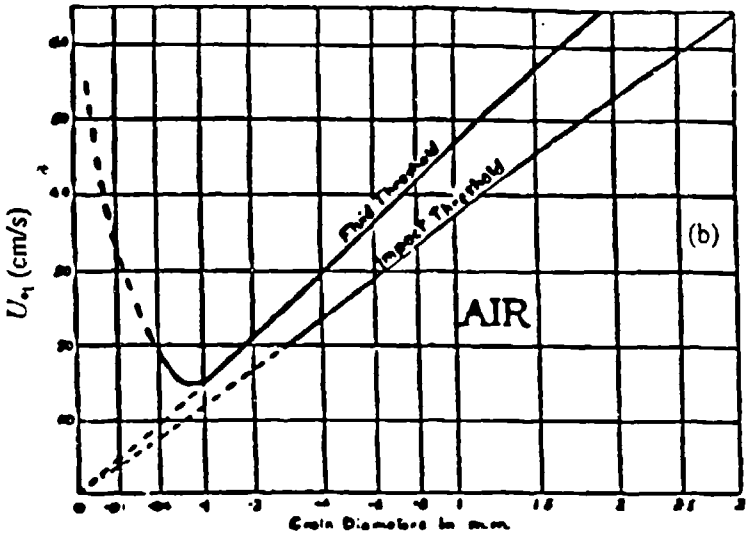

a (mm)

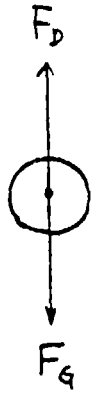

(c)

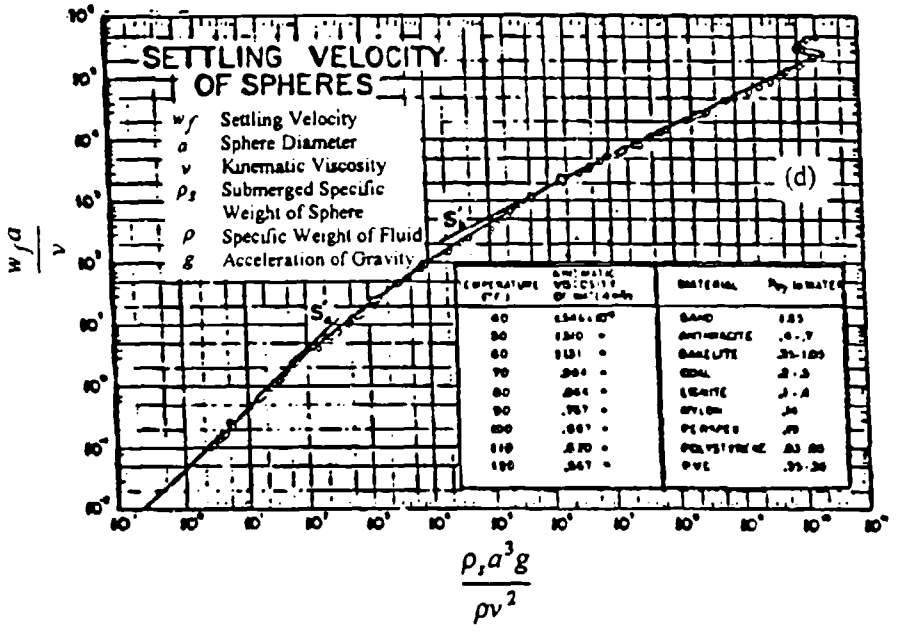

Figure 4. (a) Sketch showing the inception of particle motion subject to fluid disturbance; (b) experimental curves of the threshold friction velocity (from Bagnold, 1941, Fig. 28); (c) sketch showing the force balance of a particle falling in still air; and (d) settling velocity curve (in dimensionless form, from Yalin, 1977, Fig. 3.2).

where α is approximately the angle of repose. At the critical condition $M_G=M_D$, by equating (35) with (36), the threshold friction velocity is found to be

$$u_{*t} = \sqrt{\frac{8}{3}\frac{\tan\alpha}{A'}}\sqrt{\frac{\rho_s-\rho}{\rho}ga} = A\sqrt{\frac{\rho_s-\rho}{\rho}ga} \tag{37}$$

The experimental value for A in the case of sand transport in air is found to be approximately 0.1 for particles larger than 0.1 mm in diameter (Bagnold, 1941; Chepil, 1945). For smaller particles, the grains are not exposed to the wind flow directly but shielded under the viscous layer, and most of the wind drag is absorbed by the surface rather than the particles. Subsequently, the threshold friction velocity increases. Experimental evidence indicates that the critical diameter of such transition is at 0.08 mm (Bagnold, 1941; Chepil, 1945). In the following computation, the threshold velocity as a function of sediment diameter is digitized from Fig. 4b (reproduced from Bagnold, 1941, Fig. 28) and fitted with a polynomial function for digital computation.

Particle Fall Velocity

The terminal velocity of a particle falling in still air can be calculated by considering the balance of the grain weight and the drag force on the particle (Fig. 4c). The expressions for the two force components are the same as those given in Eqs. (33) and (34) except that in this case the flow velocity is the fall velocity, w_f, and the particle is fully exposed to air flow, thus the factor A' is unity. The resulting expression for the fall velocity is

$$w_f = \sqrt{\frac{4}{3C_D}\frac{\rho_s-\rho}{\rho}ga} \tag{38}$$

The drag coefficient C_D is a function of the Reynolds number, $Re=w_f a/\nu$, where ν is the fluid viscosity. In the laminar flow regime ($Re<1$), C_D is approximately $24/Re$, and w_f is proportional to a^2. In the turbulent flow regime ($Re>1000$), the drag coefficient is approximately constant, and the fall velocity is proportional to the square root of the grain diameter. The most frequently encountered conditions, however, fall between the two regimes, and the expression of C_D is rather complicated. Compiled from many data sets, Yalin (1977) constructed a dimensionless plot relating the fall velocity, grain diameter, and fluid viscosity (Fig. 4d). The curve is digitized and fitted with a polynomial function for numerical computation.

3.2 Results

Seven transport rate equations [Table 1, Eqs. (19) to (25)] were compared. The computed range of wind speed at 1 meter high (U_{100}) was from 2 to 40 m/s, the wind friction velocity (u_*) was up to 220 cm/s (roughness dependent), and the range of sediment diameters (a) was from 0.005 to 0.05 cm (50 to 500 μm). The complete set of computed results is presented in Figs. 5a to 5j and 6a to 6g. The following conclusions were reached from the computed results:

- Bagnold's (1941) and Zingg's (1952) equations do not contain the threshold parameter. These two equations are understood to be applicable for winds exceeding the threshold condition and may be less accurate at lower wind velocities.
- In general, the results from Bagnold's formula are near the average of all predictions. The formulas of Kawamura (1951), Lettau and Lettau (1978), and White (1979) predicted higher transport rates than Bagnold's, while Zingg (1952), Owen (1964), Iversen et al. (1976), and Schmidt (1982) predicted lower rates.

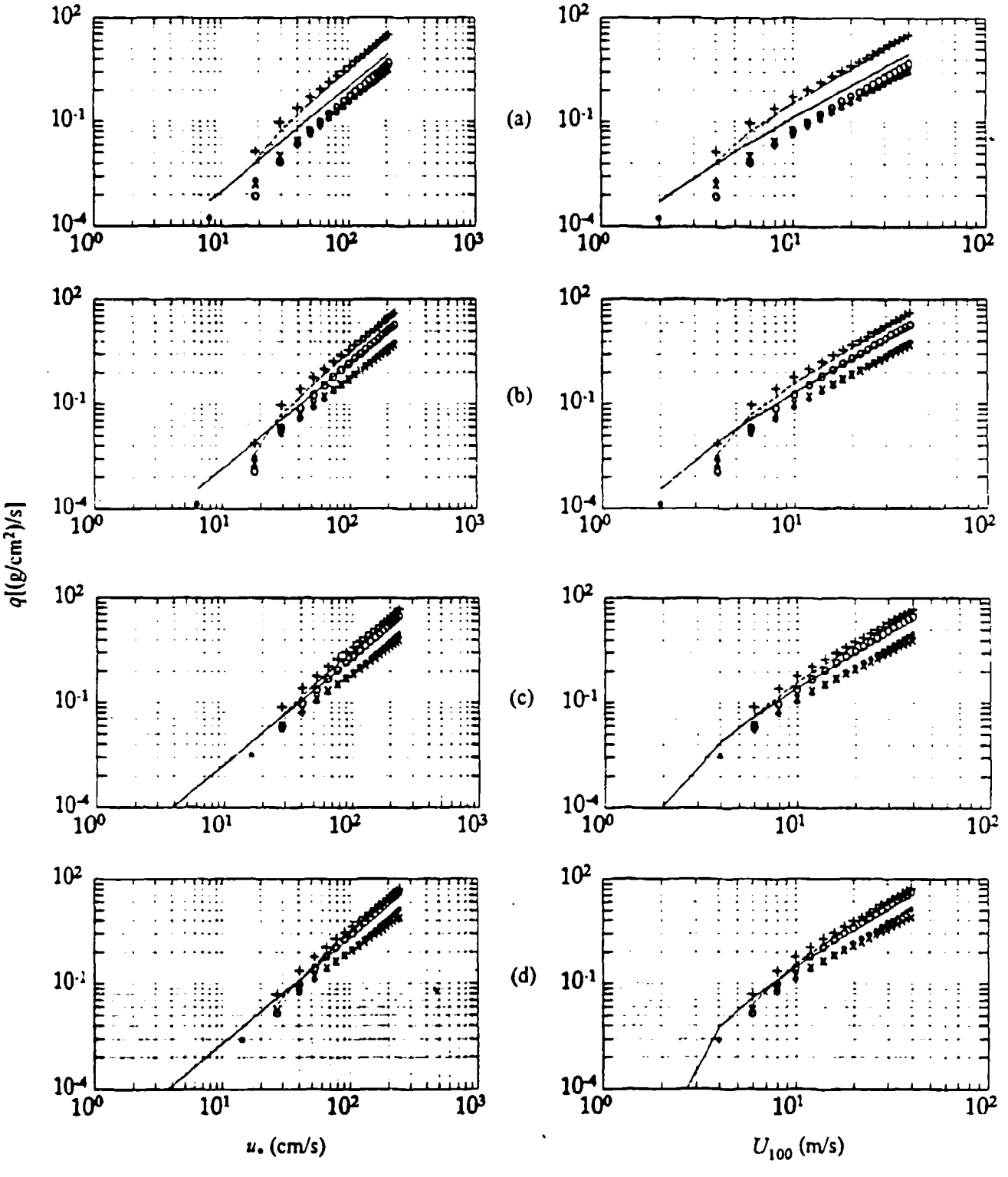

Figure 5. Transport rate as a function of wind friction velocity (left) or wind velocity (right) at 1-meter height. Equations (Table 1) suggested by Bagnold (solid curve); Lettau and Lettau (dotted curve); Kawamura (dashed curve); Iversen et al. and Schmidt (circles); and Owen (crosses) are shown for uniform sand of diameter (in cm): (a) 0.005, (b) 0.01, (c) 0.015, (d) 0.02, (e) 0.025, (f) 0.03, (g) 0.035, (h) 0.04, (i) 0.045, and (j) 0.05.

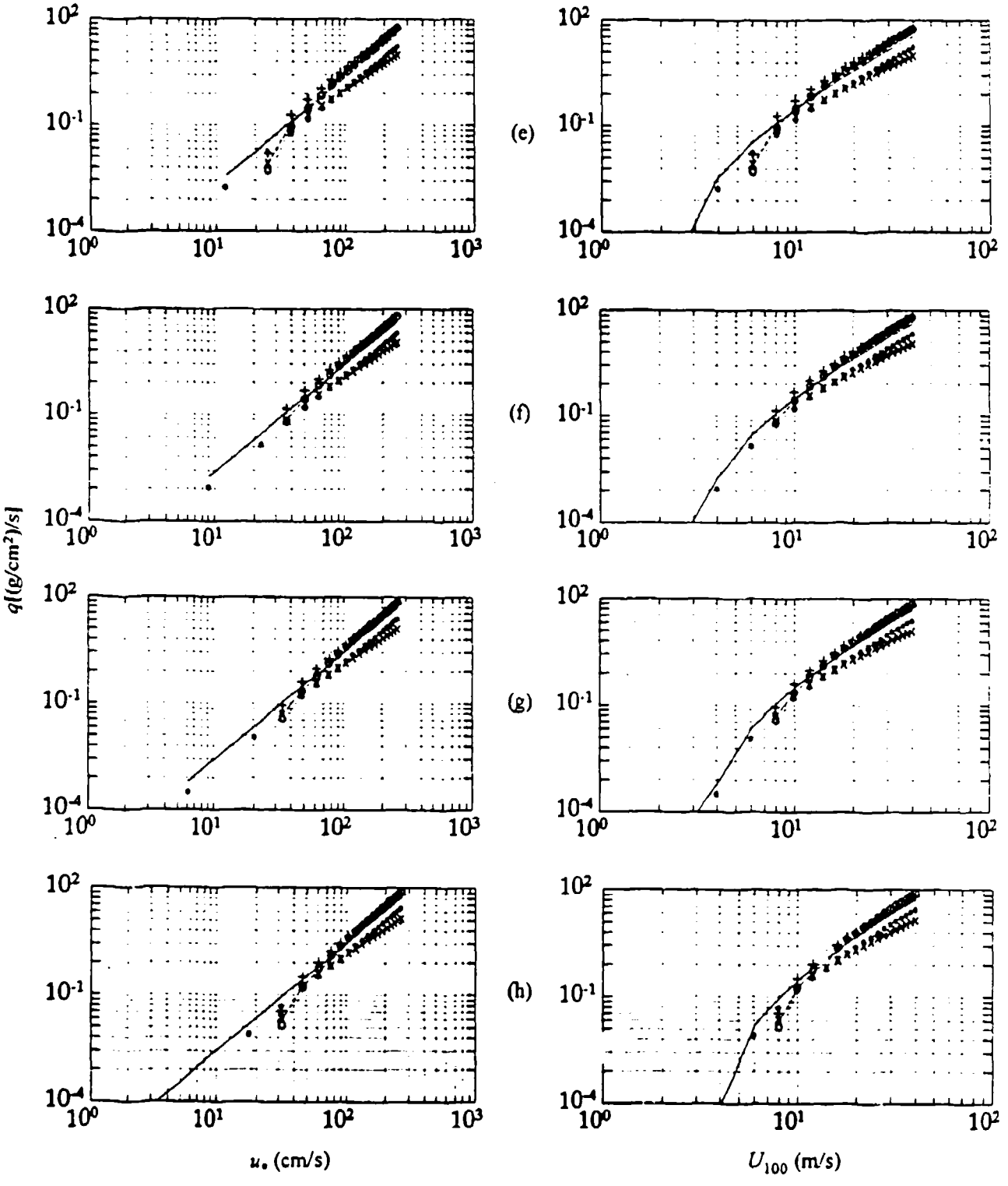

Figure 5. Transport rate as a function of wind friction velocity (left) or wind velocity (right) at 1-meter height. (Cont.)

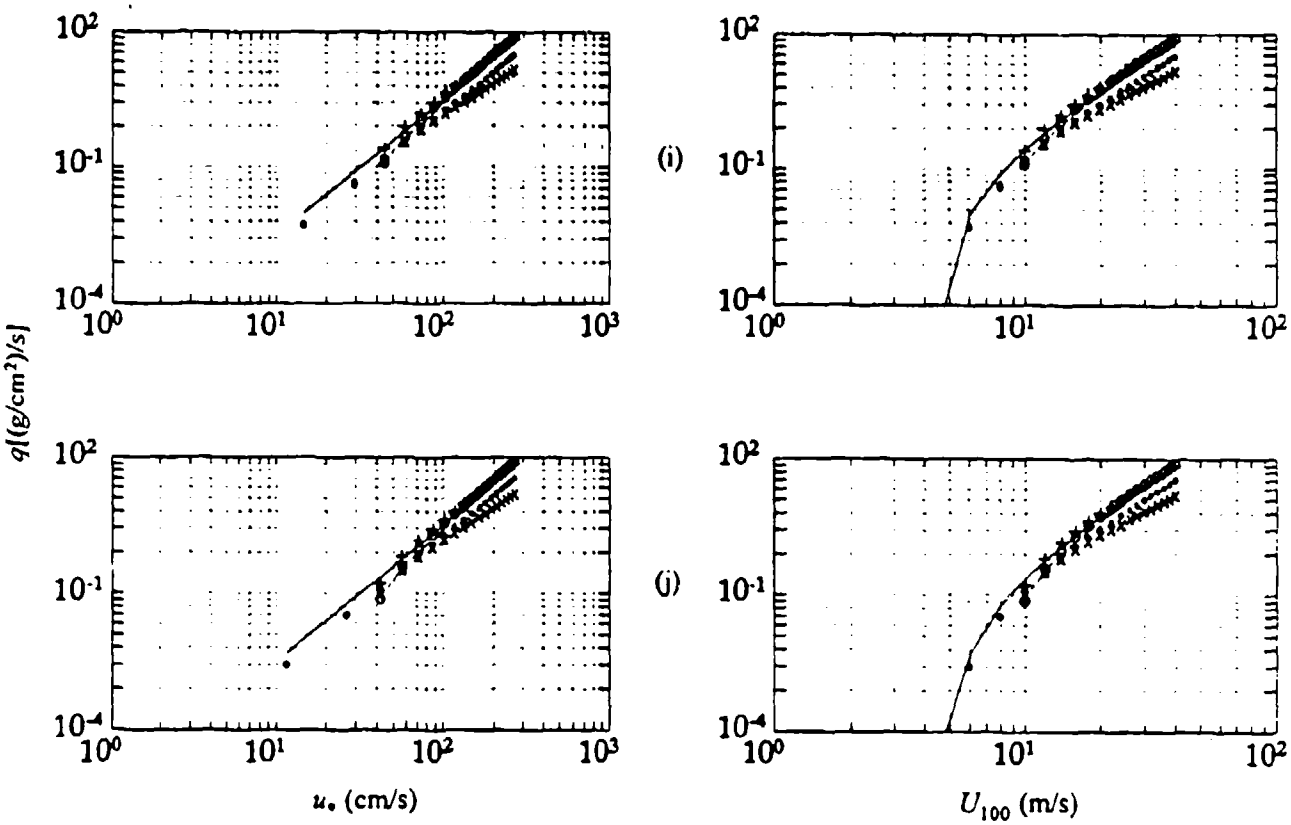

Figure 5. Transport rate as a function of wind friction velocity (left) or wind velocity (right) at 1-meter height. (Cont.)

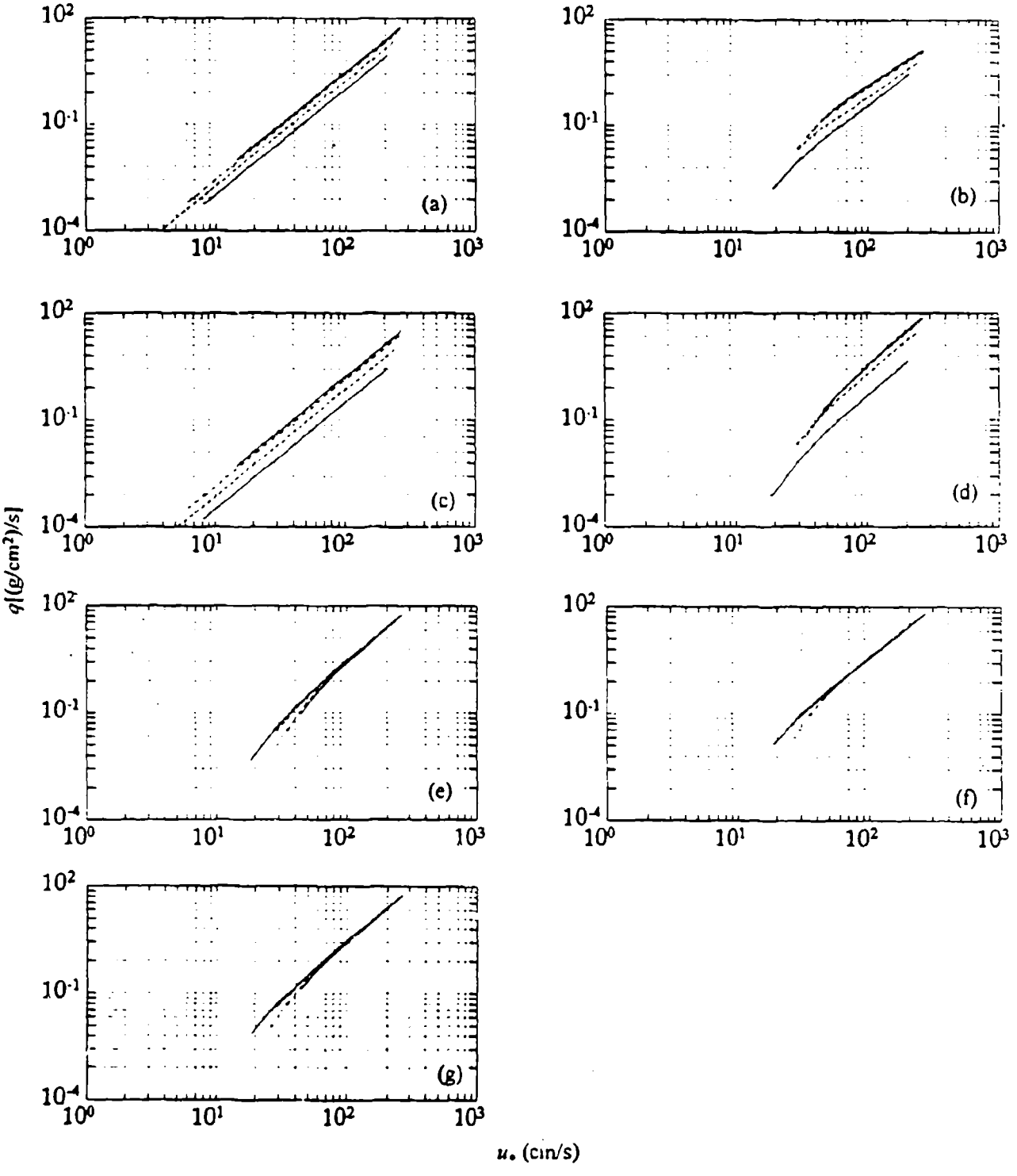

Figure 6. Calculated transport rate as a function of wind friction velocity for particle sizes from 0.005 to 0.05 cm. (a) Bagnold (1941), (b) Owen (1964), (c) Zingg (1952), (d) Iversen et al. (1976), (e) Lettau and Lettau (1978), (f) White (1979), (g) Kawamura (1951).

- The computed results agree with each other within a factor of 2 in most of the cases, except for the formula of Owen (1964), which may be off by a factor between 3 to 4 from the average at higher wind velocities. This degree of agreement is considered very good given that most of the sediment transport rate data show order-of-magnitude scatter within the individual data set and even more when different sets are combined. The large scatter occurs in both laboratory and field conditions.
- The expressions of Kawamura (1951) and Lettau and Lettau (1978) produce nearly identical results over the whole range of conditions tested. The former is somewhat more complicated.
- The degree of size dependence varies among the compared equations and can be roughly divided into two groups. Four of the seven equations show distinct size dependence (Fig. 6); these correspond to the equations that specified the particle diameter explicitly, either as a itself in the cases of Bagnold (1941) and Zingg (1952) or as the fall velocity w_f in the cases of Owen (1964) and Iversen et al. (1976).
- In the other three formulas (Kawamura, 1951; Lettau and Lettau, 1978; White, 1979), the particle size parameter is given only explicitly in the threshold friction velocity u_{*t}, which varies with particle size (Fig. 4b). All three of these equations show that the transport rate at high winds becomes independent of size; the computed results, when a ranges from 0.005 to 0.05 cm, are essentially identical for u_* exceeding approximately 80 cm/s.

In conclusion, numerical computations show that most of the sediment transport rate equations are in reasonably good agreement with each other (within a factor of 2 in most cases) over a wide range of wind velocities and sediment sizes. It is emphasized that such close agreement among various formulas is quite remarkable considering the fact that the data scatter is typically a few orders of magnitude in most reported experimental data. For the purpose of developing an algorithm to extract the size distribution information of airborne particles, the simple expression of Bagnold (1941) is selected.

Although there are several studies discussing the modification of transport rate due to particle shape factor, size distribution, and sediment density (e.g., Williams, 1964; Willetts et al., 1982; Willetts, 1983), the proposed "correction" does not appear to be conclusive for one major reason: the effects of those parameters on the wind friction velocity are significant. Much of the deviation between the transport rate/wind friction velocity observations and the basic functional form, such as that of Bagnold's, can be traced to the modification of u_*. This will be further explored in the Phase II study.

4. PARAMETERIZATION TO DERIVE THE SIZE DISTRIBUTION

To investigate the feasibility of applying the sediment transport equations to derive the number density and size distribution of particles in air, an equivalent concentration, C, was introduced. Integration over the saltation layer of the product of C and the particle convective velocity, U_p, therefore equals the sediment transport rate. Using the Bagnold transport rate equation, Eq. (12) was generated and is rewritten here

$$q = \rho \int_{z_1}^{z_2} \int_{a_1}^{a_2} \left[n(a,z) \frac{\pi a^3}{6} \right] U_p(a,z)\, da\, dz = 1.8 \left(\frac{a_m}{a_0} \right)^{0.5} \frac{\rho}{g} u_*^3 \tag{39}$$

where a_m is the median diameter of the bed material. The square bracketed term in the integrand is the equivalent concentration. To allow numerical evaluation of the vertical size distribution, a series of parameterizations is required, as is discussed in the following.

4.1 Size Range of Mobilized Sediment

The integration limits $[a_1, a_2]$ determine the size range of mobilized sediments. This range can be calculated using the threshold criterion of particle motion as reported by Bagnold (1941, see also discussion of threshold velocity in Section 3.1). As will be shown later, the effect on the outcome of the transport rate computation is strongly affected by a_2 but not a_1. The lower limit of the size integration in this feasibility study is set to zero.

4.2 Saltation Layer Thickness

The integration range $[z_1, z_2]$ represents the saltation layer thickness. The lower limit is set at the level of one sediment diameter, and the upper limit is identically the saltation height. The exact magnitude of the saltation height is not well determined. From laboratory results (e.g., Bagnold, 1936; Zingg, 1952; White and Schulz, 1977), the saltation height is typically reported to be on the order of a few centimeters, and it increases significantly with sediment diameter and slightly with wind velocity. The unrealistically low values obtained in the laboratory are due to the geometric limitation of the experimental facilities. In the open field, such as described in the reports of Bagnold (1941, p. 10) cited earlier in the Introduction, the saltation height is on the order of approximately 2 meters; it is larger for coarser surfaces and smaller when the surface is composed of fine sand. There is clearly a big gap between the field conditions and laboratory results (and the theories developed to explain the laboratory observations, such as Owen, 1964; White and Schulz, 1977). One major result of the theoretical studies of particle trajectory shows that the saltation height is closely related to the vertical component of the initial liftoff velocity, w_1. The liftoff velocity can be related to the wind friction velocity. In Owen (1964) and White and Schulz (1977), the proportionality factor derived from laboratory observations is approximately 1. Anderson and Haff (1990) suggested using $w_1=5u_*$, thus $z_2 = 25u_*^2/2g$, which is closer to the field observation value. In the subsequent computations, the last definition for z_2 is used to set the upper limit of integration. It is noted, however, that the choice of 5 as the proportionality constant appears to be arbitrary and that the resulting expression shows no dependence of saltation height on sediment diameter, against the observational evidence described earlier. Further improvement is needed in the future.

4.3 Convective Velocity

The convective velocity $U_p(a, z)$ is assumed to be the wind velocity, $U(z)$:

$$U(z) = 2.5u_* \ln\left(\frac{z}{z_0} \right) \tag{40}$$

where the dynamic roughness is calculated using the formula $z_0=0.02065u_*^2/2g$ (Owen, 1964; Anderson

and Haff, 1990). There are few reports on the parameter $U_p(a, z)$, but the numerical computation of Anderson (1986, p. 27) appears to support that U_p is proportional to U over an extended elevation.

4.4 Vertical Distribution and Shape Factor

The function $n(a, z)$ is expressed as

$$n(a,z) = Kn(a)f(z) \tag{41}$$

where K is a scaling factor and the functions $n(a)$ and $f(z)$ are the "shape factors" with respect to size and elevation. From extensive research, it was established that $f(z)$ attenuates vertically following either an exponential law, a power law, or a combination of both. In either case, the z-integration can be carried out explicitly. Similarly, there are a few choices of $n(a)$. The two most frequently adapted distribution forms are the log-normal and power law. Depending on the functional forms specified, the scaling factor K in Eq. (41) can be derived from Eq. (39). The integrated concentration of airborne particles within a defined volume can then be calculated (see Section 2.4). To illustrate the procedure to derive size distribution from the transport rate equation, assume

$$f(z) = (z/z_r)^{-m} \tag{42}$$

where z_r is a reference elevation,

$$n(a) = (a/a_m)^r \tag{43}$$

the exponent $r=s$ for $a/a_m<1$ (Region I) and $r=-l$ for $a/a_m>1$ (Region II), where both s and l are positive real numbers. Observational evidence exists showing that the exponent s in Region I (the small-particle region) is somewhat invariant (e.g., Bagnold, 1941, Figs. 41, 44) at various stations of sampling. The exponent l in the large-particle region is usually larger (shape is steeper) at higher elevations or further downstream of the sediment source. The median size, a_m, of the airborne particles may also vary with elevation and wind condition. Functional expressions for the variation of l and a_m with z or u_* are not available at this stage, but data from Bagnold (1941), Chepil and Woodruff (1957), Williams (1964), and Nickling (1975, 1978, 1983) contain reports on the size distribution at different elevations and can be used for establishing the relationship. At the present, the parameters l and a_m are treated as constants.

4.5 Analytical Expression

With the above parameterization, the remaining unknown variable is the scaling factor K of the size distribution function. By choosing a sediment transport rate equation (such as the Bagnold's transport rate equation), the solution for K can be expressed in analytical form

$$K = \frac{0.72(a_m/a_0)^{0.5}\left(u_*^2/g\right)}{I_z I_a} \tag{44}$$

where

$$I_z = \frac{1}{m+1}\left[z_2^{m+1}\ln\frac{z_2}{z_0} - z_1^{m+1}\ln\frac{z_1}{z_0}\right] \tag{45}$$

$$I_a = \frac{1}{s+4} + \frac{\left(0.046\dfrac{u_*^2}{ga_m}\right)^{4-l} - 1}{4-l} \tag{46}$$

and $z_0=0.02065u_*^2/2g$, $z_1=a_m$, and $z_2=25u_*^2/2g$, as defined earlier.

5. RESULTS OF SENSITIVITY TESTS

To allow numerical evaluation of the vertical size distribution, a series of parameterization formulas is required. The relevant parameters include wind friction velocity u_*, threshold friction velocity u_{*t}, fall velocity w_f, size range of mobilized sediment $[a_1, a_2]$, saltation layer thickness $[z_1, z_2]$, convective velocity $U_p(a, z)$, and the functional representation of $n(a, z)$ by $Kn(a)f(z)$. For the purpose of demonstrating the feasibility of obtaining the number density and size distribution from the transport rate equations, a series of analytical expressions was established for the various parameters, based on physical considerations and available data comparison. Sensitivity tests were performed to evaluate and rank the factors that affect the outcome of computed number density of airborne particles. A set of computational results are presented in Figs. 7 through 9. The captions provide detailed discussions of these results. Some conclusions are summarized in the following:

- The major contribution of the transport is from the large particles (Region II, $a>a_m$). This is because the weight of transported material is proportional to the volume, which is proportional to a^3 [see panel (iv) of Figs. 7 through 9; the contribution from Region II is denoted with o and the total contribution is plotted as x].
- Because the transport rate is dominantly contributed by larger particles, the variation with the large particle distribution, as represented by the parameter l, is significant. Notably, for a narrow size distribution ($l>3$), as u_* increases, the size range of mobilized particles and the number density increase [Fig. 7a(i) and (ii), symbol o]. However, if the distribution is broad (Fig. 7b) while the size range still increases with increasing wind, the number density may actually decrease. This is due to the fact that the motion of a particle derives its momentum from the wind. If the size distribution is broad, the number of larger particles mobilized is proportionally increased as compared to the case of a narrow size distribution. Thus, the total number of particles needed to reach equilibrium with wind is less for a broad size distribution. Computation shows that $l=3$ represents a critical condition (Fig. 8a) at which the total number of particles mobilized, N, is more or less independent of the wind friction velocity (but the representative size of the airborne particles increases as the wind velocity increases, see next entry). For narrower distribution ($l>3$), N increases monotonically with u_*; for broader distribution ($l<3$), N decreases as u_* increases.
- Another useful indicator of the size distribution of airborne material is the representative particle size. There are a few different ways to represent the particle size: the linear dimension, a_1, such as the diameter of spherical particles or the axial lengths of irregularly shaped particles; the square root of the cross-sectional area, a_2; or the cubic root of the volume, a_3. Each expression has its own significance in remote sensing applications. For example, a_1 is relevant in measuring the transit time of a particle passing through a given distance; a_2 is relevant to the measurement of cross sections such as scattering and visibility; and a_3 is related to properties such as volume absorption and mass concentration. As shown in panel (iii) of Figs. 7 through 9, the characteristics of a_i, $i=1$, 2 and 3, are very sensitive to the various parameters specified, especially the exponent l. Such characteristics can be used to develop methods of identifying the size distribution of airborne particles by combining output from different sensors.
- The effect of the vertical decay function, represented by the parameter m, is also significant. At this stage, it is found that the computational range (in terms of the wind friction velocity) can be seriously limited for a particular value of m. For example, if $m=1.1$, no computational difficulties were encountered for u_* up to 200 cm/s; when $m=2$, it was found that the computation broke down near $u_*=80$ cm/s (see Figs. 8a, 8b, and 8c; the parameters are identical to those of Figs. 7a, 7b, and 7c except m). The coding of the computational programs and the parameterization functions can be improved to expand the range of applications.

Figure 7. Case studies of number density and size distribution analysis derived from sediment transport rate equations. Plots (a), (b), and (c) are presented to show the effect of parameter l (the exponent of the shape function of large particles) on various aspects of the airborne particle properties. The other parameters are $z_0=0.02065u_*^2/(2g)$; $z_2=(5u_*)^2/(2g)$; $a_m=0.025$; $s=4.1$; $m=1.1$. All units are in cgs. In each plot, there are four panels, (i) through (iv), as defined below.

(i) The normalized particle size distribution computed with u_* at 20, 40, 60, ..., 200 cm/s. The increase of the size range of mobilized particles at greater u_* is revealed by the broadening of the distribution curves. Compare panels 7a(i) and 7b(i), it is seen that in the former case (narrow distribution in the source material), as wind increases, the airborne particles increase monotonically. However, if the distribution of the source material is broad as in the latter case, although the size range of particles mobilized still increases monotonically, it takes fewer saltation particles per particle size-division to "absorb" the wind momentum because the airborne particles in this case are larger. The critical "broadness index" is $l=3$, at which the number per size-division remains approximately invariant with wind [panel 7c(i)].

(ii) The scaling coefficient, K, of the number density distribution (x), and the total number, N, of particles integrated over the size range (o), plotted as functions of wind friction velocity. These plots give a more direct apprehension of the discussion presented in (i). For the two lowest wind velocities, the magnitudes of both K and N are similar in the three panels 7a(ii), 7b(ii) and 7c(ii) because the mobilized particles are mainly of small size, the distribution function in the small particle region for the three computations was identical (i.e., $s=4.1$). As wind increases, more large particles are sent into the air, and the composition of airborne particles is affected by the size distribution of the large particles in the source material. In general, the total number of particles is expected to increase with wind, such as in panel 7a(i). However, if the supply of larger particles is abundant, that is, broad distribution in the source function, the total number may actually decrease with increasing wind because the broadening of the mobilized size range introduces more large particles (as compared to the case of narrow-distribution source material) to absorb the increased wind momentum. Because of the presence of more large particles, the total number of airborne particles required to reach an equilibrium with wind is actually reduced. The critical broadness index is $l=3$ [panel 7c(ii)], at which the total number of particles airborne is maintained approximately constant.

(iii) As a result of the difference in the source material (i.e., l), the composition of airborne particles can be quite different under identical wind condition. A useful index to denote the airborne particle composition is the representative size, which can be the linear size, computed as the first moment of size distribution function a_1 and plotted as the lowest curve in these panels, the square root of the cross-sectional area, computed as the square root of the second moment a_2 and plotted as the middle curve, or the cubic root of the volume, computed as the cubic root of the third moment a_3 and plotted as the top curve. For narrow-distributed source material, the variation of a_i, $i=1$, 2, and 3, at different wind conditions is small [panel 7a(iii)]; for broad distribution, the representative size can be significantly different at different wind velocities [panels 7b(iii) and 7c(iii)].

(iv) This panel shows the contribution to the momentum balance from the large particle region (o) as compared to the total (x). It is seen that except at the very low wind condition, where only small particles are mobilized, the contribution from large particles dominates the momentum balance between wind and sediment.

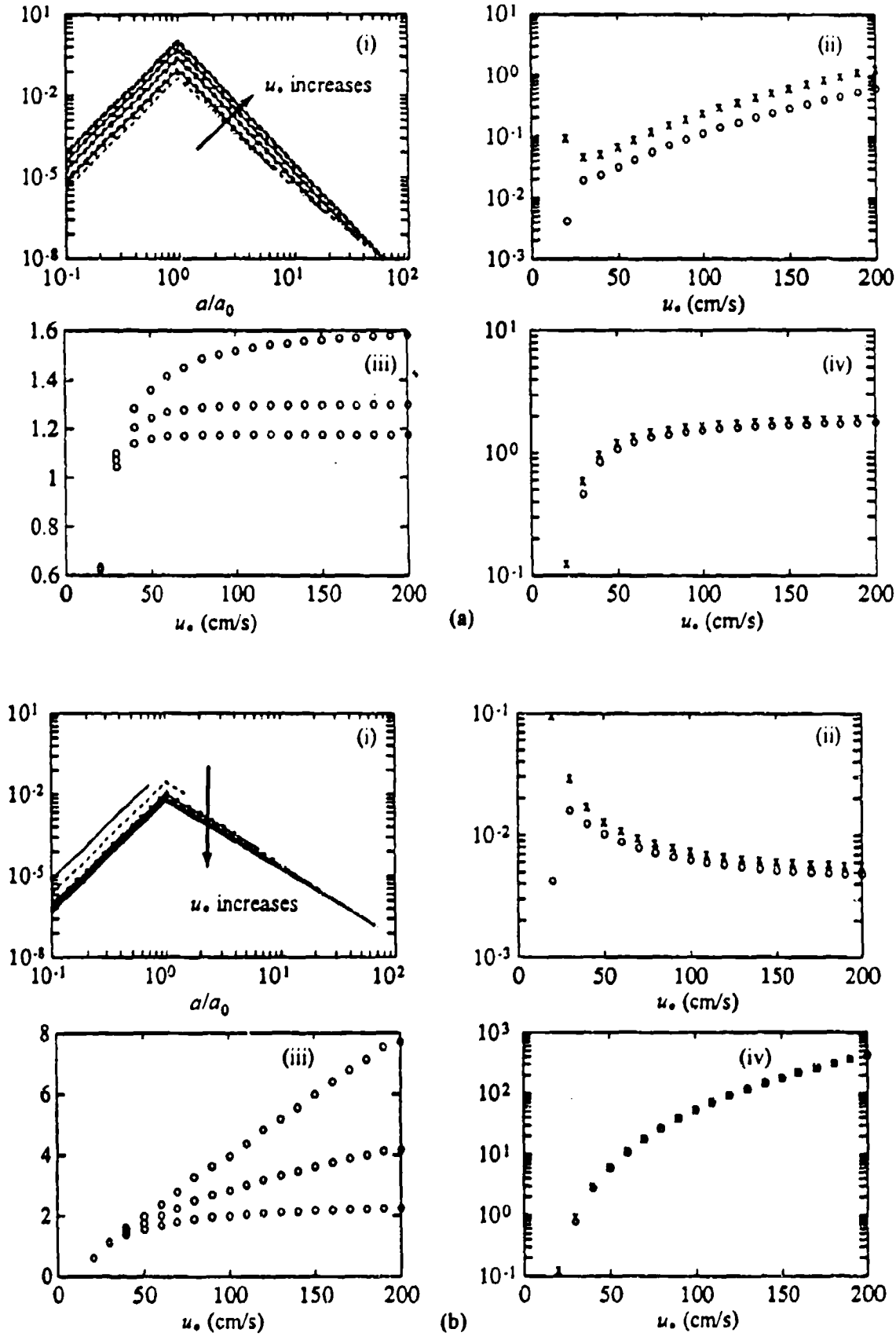

Figure 7. Case studies of number density and size distribution analysis derived from sediment transport rate equations. (Cont.)

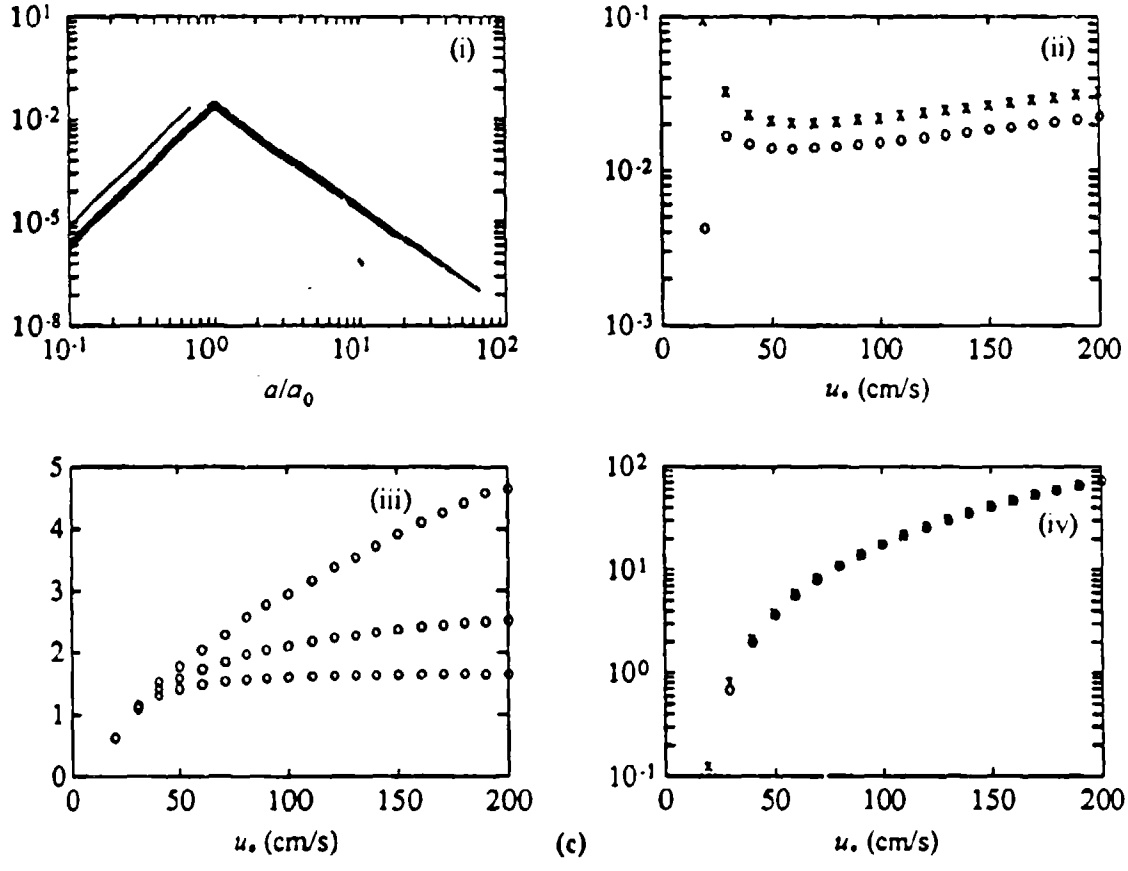

(c)

Figure 7. Case studies of number density and size distribution analysis derived from sediment transport rate equations. (Cont.)

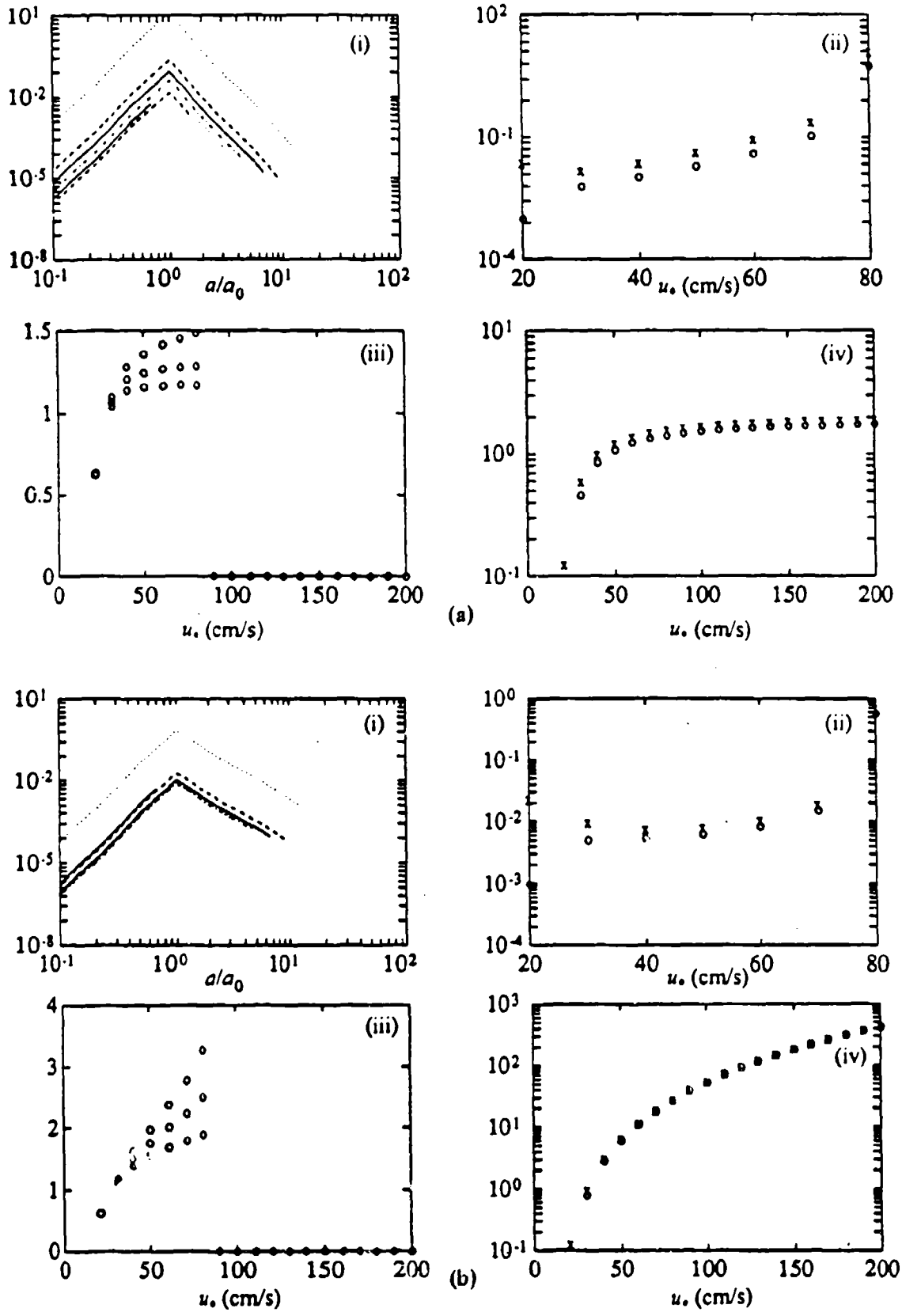

Figure 8. Case studies showing the effect of the vertical decay function, represented by the exponent m of the function $f(z)=z^m$. Plots (a), (b), and (c) are computed with identical parameters as those shown in Fig. 7 except that m=2. The plotted properties in panels (i), (ii), (iii), and (iv) are the same as in Fig. 7. Because of the problem of a singularity, the computation range of u_* in this figure is 20 to 80 cm/s.

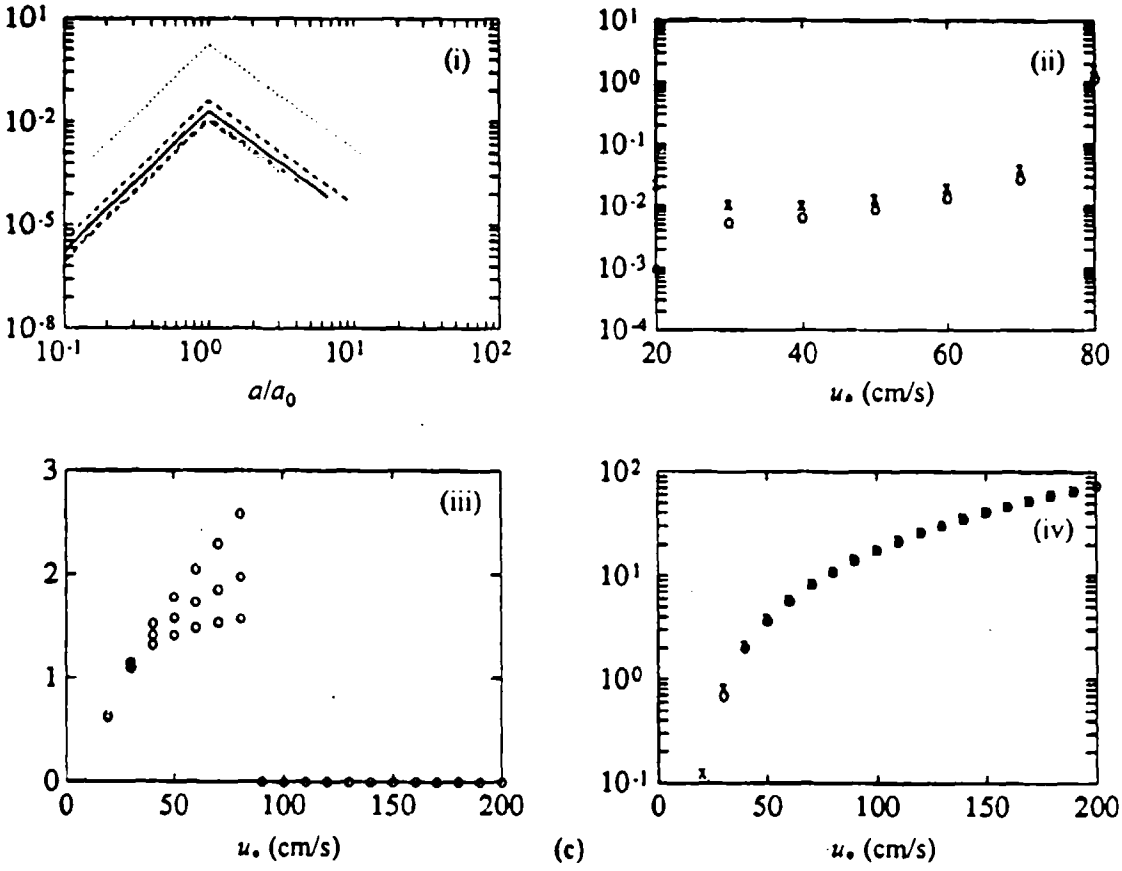

Figure 8. Case studies showing the effect of the vertical decay function, represented by the exponent *m* of the function $f(z)=z^{-m}$. (Cont.)

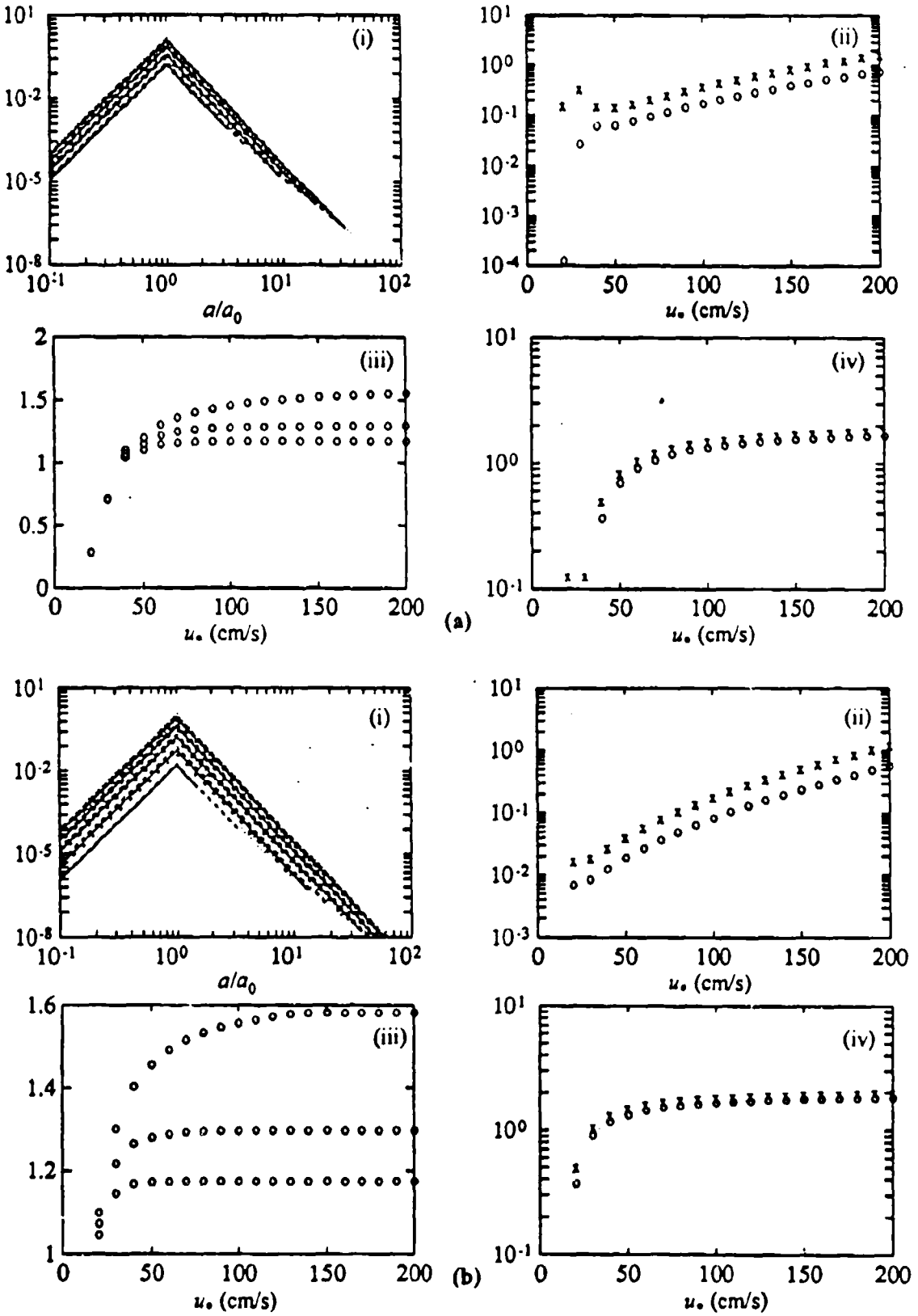

Figure 9. Case studies showing the effect of the median diameter of the source material, as represented by the parameter a_m. (a) a_m=0.05 cm; (b) a_m=0.0125 cm. The reference condition is Fig. 7a, a_m=0.025 cm. The most obvious effect due to this parameter is in the rate of increase of particle numbers as a function of wind [compare panels 9a(ii) with 9b(ii) and 7a(ii)]. The smaller the median diameter, the faster the rate of increase.

The effect of the median size of particles on the number density is shown in Figs. 7a, 9a, and 9b, in which, s, $!$, and m are identical and only a_m is varied (0.025, 0.05, and 0.0125 cm, respectively). The rate of increase of the particle number with the wind friction velocity is found to be reduced as a_m increases [compare panel (ii) of the three figures]. This result, again, is a consequence of the momentum balance governing the dynamics of saltation and wind flow. The wind momentum is transferred to particles through the drag force, which is proportional to a^2; the mass of particles is proportional to a^3. For the same increment of wind velocity, the increased momentum is balanced by a given mass of saltation particles, which can be from a large number of small particles or a small number of large particles. Accordingly, the rate of increase in the number of airborne particles decreases as the particle size increases.

6. DISCUSSION

6.1 Integrated Number Density and Angle of Incidence

In the lower boundary layer near the ground, the vertical gradient of airborne particle distribution is large. Therefore, the integrated number of particles inside the propagation path of a target acquisition system is strongly dependent on the incident angle. Qualitatively, it is expected that the number of particles at a grazing angle will be considerably larger than those in the more zenith-looking configurations. The spherical coordinate system is used to obtain the integrated number of particles within the propagation path. With the assumption that the horizontal distribution of airborne particles is relatively uniform and that the vertical distribution can be expressed as $f(z)=z^m$, the integrated number of particles within a pencil beam was plotted in Fig. 2. The results show that the particle number increases drastically as the incident angle increases beyond approximately 60°. Depending on the vertical gradient of particle distribution, it is not uncommon to see a few orders of magnitude increase from a 10° to an 80° incident angle. The large increase of airborne particles in the propagation path can cause serious deterioration of system performance.

6.2 Transport Rate Equations

It is surprising to see that of the many forms of sediment transport rate equations, the calculated results are in close agreement with each other, in most cases within a factor of 2 (Fig. 5). This is truly amazing considering that the coefficients of those equations are usually derived from fitted data from various sources ranging from well-controlled laboratory experiments to complicated field conditions, of which, order of magnitude data scatter is typical. These equations can be roughly divided into two major categories (Fig. 6). The first kind shows distinct size dependence, such as the equations of Bagnold (1941), Zingg (1952), Owen (1964), and Iversen et al. (1976). In these equations, the sediment size is explicitly incorporated either directly as a or as w_f, the fall velocity. In the second category, the dependence of the calculated transport rate on sediment size is implicitly incorporated in the threshold velocity parameter. Computational results indicate that the effect on the transport rate is much weaker, especially at higher wind velocities. The equations of Kawamura (1951), Lettau and Lettau (1978), and White (1979) fall into the latter category. Most recent equations incorporate the threshold friction velocity u_{*_t} in the formulation to ensure that there is no transport rate at winds less than the threshold magnitude. The equations of Bagnold (1941) and Zingg (1952) do not explicitly specify the threshold friction velocity in the formulation. These equations are understood to be applicable only at $u_* > u_{*_t}$. Although equations without u_{*_t} are likely to produce larger errors at lower wind velocities, Bagnold's equation is chosen for the development of the algorithm to derive size distribution from the transport rate equations, due to its simplicity and sound physical basis of derivation. The resulting algorithm, however, can easily be modified to adapt other transport rate equations.

6.3 Size Distribution and Sediment Flux Formulation

The results from the sensitivity tests, as outlined in the last section, demonstrated that the number density of airborne particles can be derived from the transport rate equations. Because of the large number of factors involved in the sediment transport process, the critical step to an accurate prediction of the particle number density is the parameterization procedure. As expected, some of the factors are better understood than others. For example, the threshold condition is more or less established and the size range of particles to be mobilized can be derived as a consequence. On the other hand, our understanding of some other factors such as the variation of z_2, m, i and a_m with respect to z and u_* is only qualitative. A more quantitative relationship can only be derived from experimental data or numerical simulations of the sediment saltation process. A small set of experimental data and numerical results has been collected during the course of this

research. These include the laboratory data of Bagnold (1936), Zingg (1952), Williams (1964), Willetts et al. (1982), and Willetts (1983); field data of Hsu (1971, 1973), Gillette and Blifford (1972), Gillette and Walker (1977), and Nickling (1975, 1978, 1983); and numerical simulations of Anderson (1986), Anderson and Hallet (1986), Anderson and Haff (1988), and Werner (1987, 1990). The present parameterization scheme can be improved with the augmentation of the above data sets. However, it is realized that all the data sets are limited to particular environmental conditions, and continuous expanding of the data base is important. Also, impressive progress was made during the last few years on the numerical simulation of eolian transport processes by Anderson, Haff and their co-workers (see Haff and Anderson, 1989, and Anderson and Haff, 1990, for a more detailed discussion). It is very promising that with a concerted effort, we would be able to establish a reasonable range of each less-understood parameter. From such information, the possible range of integrated particle number densities within the propagation path can be computed.

7. RECOMMENDATIONS

Based on this feasibility study, it is concluded that the number density of the saltation particle size distribution can be derived from sediment transport rate formulas. From our comparison study, it is found that the numerical difference among formulas of various complexities is small compared to the scatter of experimental data. For the purpose of developing the algorithm of the size distribution function, simpler formulas are sufficient.

Results from the sensitivity tests indicate that the number density of saltation particles is critically controlled by the parameters $z_2(a, u_*)$, $m(a, u_*)$, $l(z, u_*)$, and $a_m(z, u_*)$. In the feasibility study, a simple parameterization scheme was used to reach an analytical solution. The parameterization can be improved based on physical considerations and experimental data (e.g., Bagnold, 1936, 1941; Zingg, 1952; Chepil, 1957a, 1957b; Williams, 1964; Hsu, 1971, 1973; Gillette and Blifford, 1972; Gillette and Walker, 1977; Nickling, 1975, 1978, 1983; Horikawa et al., 1983, 1984, 1986). Reanalysis of these data sets may provide the necessary functional relationship and the likely range of variation of each parameter. Thus the upper and lower limits of airborne particles can be calculated for output to the application programs or target acquisition systems to enhance their performance. Of these data sets, the laboratory results of Williams (1964) and the field data of Nickling (1975, 1978, 1983) provided detailed documentation of the size distribution as functions of elevation and wind friction velocity and appear to be most promising for our purpose of establishing the parameterization functions.

Williams (1964) investigated the variation of size distribution of sedimentary particles at five elevations (0.5, 2.5, 5.5, 9.5 and 15.5 cm) in a wind tunnel 9.14 m long with a 35.5 x 35.5 cm cross section. Three different types of particles (spheres, sand grains, crushed quartzite) with three initial size distributions (uniform, symmetrical, and truncated) were uses as the base samples. Experimental runs at three wind intensities (approximate u_* = 38-50, 78-92, and 117-135 cm/s) were conducted with each sample; thus, a combination of 27 cases were obtained. The size distribution at each elevation as well as the first three moments, representing the mean diameter, sorting factor, and skewness, were reported. From the data set, Williams also computed the vertical distribution of sediment concentration, reported to decay exponentially, and transport rate, varying as a power of u_*, with the exponent being 2.7 for crushed quartzite, 3.4 for sand, and 4.1 for spheres. Detailed results including the size distribution, mean diameter, sorting factor, and skewness, all as functions of wind and elevation, as well as the vertical distribution of sediment concentration, were presented in graphic form in the original paper. The data set, with all the detailed measurements, will serve as our fundamental database of parameterization. However, due to facility limitations, the vertical scale of laboratory data sets is typically 1 to 2 orders of magnitude smaller than the field conditions (for example, the saltation height in laboratory experiments is typically a few centimeters, while in the field, the top of the saltation layer is 1 to 2 m). Field data and numerical simulation may help the extrapolation of laboratory data to field conditions.

The field results of Nickling (1975, 1978, 1983) include data of creeping (by an underground trap), saltation (collected by a wind-vane trap with an orifice 1 m high, 1 cm wide, and the lower edge 0.05 cm above surface), suspension (by drawing air samples through filters), and wind velocity distribution at eight elevations (0.5, 1, 1.5, 2, 4, 6, 9, 12 m). The ground samples were collected regularly. The statistical properties of the size analysis of most of the samples were also reported. Over a period of two months, fifteen storm events were encountered. Results on the relative contribution of creeping, saltation, and suspension to the total transport rate, wind dependence, mean size, sorting factor, skewness of suspended samples at all heights, and the effect of moisture and salt concentration on the transport rate were documented in great detail. The field data set of such details is rather unique and very precious. However, the experimental site is a river delta with very limited size variability, and the atmospheric stability condition appears to be predominantly unstable. Because of the fine sand size (median diameter approximately

60 μm), the contribution of the suspension load to the total transport is relatively large, more than 60% in 4 of the 15 storm cases (as compared to 20% in the case of regular dune sand, Bagnold, 1941).

Not to be overlooked is the work of Bagnold, summarized in his classic book *The Physics of Blown Sand and Desert Dunes* (1941). In a slightly different context, Bagnold investigated the size distribution of saltation sediment, including the mean distribution, the temporal variation during unsteady wind episodes, and spatial variation over nonuniform surfaces. It was found that the size distribution at any stage can be expressed as a power law $n(a)=(a/a_m)^r$, where the exponent $r = s$ in the small size region (Region I, $a<a_m$), and $r = -l$ in the large size region (Region II, $a>a_m$); both s and l are positive numbers. It is quite interesting to see that the shape function in Region I remains relatively constant and resembles closely that of the source material. This property is important for our development of the transition between saltation to suspension at the top of the saltation layer. The shape factor in Region II is not as constant, showing dependence on wind and space or time.

In order to establish parameterization to cover a wide range of source material parameters, a more extensive database will be needed. There have been many data sets reported in the sediment literature of different degrees of environmental parameter measurements and different levels of data analysis details. Careful classification and a cataloging system need to be established at an early stage to make efficient use of these precious data sets. In any event, the writer is confident that there are sufficient research results for establishing a reasonable range for each parameter of interest. For the established range, the upper and lower limits of the number of saltation particles under given wind and soil conditions can be defined. Program output can also include information such as the most likely condition, worst- and best-case scenarios, confidence interval and other statistics useful to the system operations and decision making.

Due to the time limit, only the theoretical aspects of the turbulent suspension process were reviewed. Because fine dust can reach a much higher altitude, the effects to the military operations can be significant. Luckily, our understanding of the suspension process is much more satisfactory. The data agreement on the vertical distribution with various theories is considerably better than the saltation counterpart, although the absolute magnitude remains a difficult quantity to parameterize. Saltation, occurring at the lower region of the boundary layer, serves as the boundary condition of suspension. From continuity consideration, the reference concentration of suspension can be set to equal the saltation "concentration" at the top of the saltation layer. The concept of matching saltation and suspension needs to be tested further with experimental data.

With the parameterization procedure established, programming of the numerical procedure to generate results of number density and size distribution and the application programs designed for end users can proceed. The major program elements and application considerations are:

- Develop numerical integration subroutines (quadrature) such that the computational procedure can handle more complicated parameter functions.
- Apply the saltation results to the suspension component of the sediment transport process. Saltating particles impact the surface and dislodge small dust particles that can be suspended into high elevations and stay aloft for a long period of time. The suspension component is important in determining the visibility and image obscuration at high elevations.
- Develop the coordinate transformation program to obtain the integrated number of particles in the propagation path of target acquisition systems. Generate results in graphic, tabular, and computer data file formats for interfacing with other remote sensing applications or additional processing.
- Develop the algorithms that relate the calculated particle size concentration to visibility, transmittance, absorption, and scattering of the visible to infrared optical spectrum, as well as millimeter radar wavelengths, using the Mie scatter programs available at QUEST (courtesy of Dr. Yogesh C. Agrawal).

- Generate application programs on a PC notebook computer to generate integrated number and size spectra of particles within the path of target acquisition systems for field operation.
- Compare the numerical output with laboratory and field data. Design and carry out field operation and data analysis in coordination with the sponsor.
- Design automatic and manual modes of computation. In the former, the program requests only minimum input parameters such as estimates of wind speed and soil type. The program will generate results based on a set of prestored parameters to provide information on the most likely conditions, worst-case and best-case scenarios, and assorted statistics to assist field operations. Manual mode is more suitable for the situation when more detailed environmental measurements are available and is useful for planning, forecasting, and hindcasting.
- The application programs will be designed to be operated on a PC notebook-based, field-grade computer. User-friendliness is a major consideration in the design. The program can be run either in Q&A mode or it can be menu driven. Results will be presented in the format of graphics, tabulation, and digital files for communication to another system.

Undoubtedly, this list of elements will grow as the research progresses. We will maintain continuous communication with the sponsor to update and improve the program design during the course of Phase II study.

ACKNOWLEDGMENT

This research is sponsored by the U.S. Army Research Laboratory, Battlefield Environment Directorate, through the Small Business Innovation Research (SBIR) Program under Contract No. DAAL06-92-C-0010. Mr. Frank V. Hansen is the Technical Monitor.

REFERENCES

Anderson, R. S., Sediment transport by wind: Saltation, suspension, erosion and ripples, Ph. D. Dissertation, Dept. Geological Science, U. Washington, 1986.

Anderson, R. S. and B. Hallet, Sediment transport by wind: toward a general model, *Geol. Soc. Am. Bull.*, 97, 523-535, 1986.

Anderson, R. S. and P. K. Haff, Simulation of eolian saltation, *Science*, 241, 820-823, 1988.

Anderson, R. S. and P. K. Haff, Simulation and suspension of particulate matter in air, Final Rep., US Army Research Office DAAL03-89-K-0089, 1990.

Bagnold, R. A., The movement of dessert sand, *Proc. R. Soc.*, A157, 594-620, 1936.

Bagnold, R. A., *The Physics of Blown Sand and Desert Dunes*, Methuen, London, 1941.

Chepil, W. S., Dyna ics of wind erosion: II. Initiation of soil movement, *Soil Sci.*, 60, 305-320, 1945.

Chepil, W. S., Sedimentary characteristics of dust storms: I. Sorting of wind-eroded soil material, *Am. J. Sci.*, 255, 12-21, 1957a.

Chepil, W. S., Sedimentary characteristics of dust storms: . Composition of suspended soil, *Am J. Sci.*, 255, 104-114, 1957b.

Chepil, W. S., and N. P. Woodruff, Sedimentary characteristics of dust storms: II. Visibility and dust concentration, *Am. J. Sci.*, 255, 104-114, 1957.

Clift, R., J. R. Grace, and M. E. Weber, *Bubble Drops and Particles*, Academic Press, New York, 1978.

Dyer, K. R., and R. L. Soulsby, Sand transport on the continental shelf, *Ann. Rev. Fluid Mech., 20*, 295-324, 1988.

Gillette, D. A. and I. H. Blifford, Measurements of aerosol size distributions and vertical fluxes of aerosols on land subject to wind erosion, *J. Appl. Meteor.*, 11, 977-987, 1972.

Gillette, D. A. and T. R. Walker, Characteristics of airborne particles produced by wind erosion of sandy soil, High Plains of West Texas, *Soil Sci*, 123, 97-110, 1977.

Greeley, R. and J. D. Iversen, *Wind as a Geological Process on Earth, Mars, Venus and Titan*. Cambridge Univ. Press, Cambridge, 1985.

Haff, P. K. and R. A. Anderson, Saltation and suspension of particulate matter in air, Final Rep. USARO, DAAL03-86-K-0132, 1989.

Horikawa, K., *Coastal Engineering*, University of Tokyo Press, 1978.

Horikawa, K., S. Hotta, S Kubota and S. Katori, On the sand transport rate by wind on a beach, *Coast. Eng. Japan*, 26, 101-120, 1983.

Horikawa, K., S. Hotta, S. Kubota and S. Katori, Field measurement of blown sand transport rate by trench trap, *Coast. Eng. Japan*, 27, 213-232, 1984.

Horikawa, K., S. Hotta and S. Kubota, Field measurement of vertical distribution of wind speed with moving sand on a beach, *Coast. Eng. Japan*, 29, 163-178, 1986.

Hsu, S. A., Wind stress criteria in eolian sand transport, *J. Geophys. Res.*, 76, 8684-8686, 1971.

Hsu, S. A., Computing eolian sand transport from shear velocity measurements, *J. Geol.*, 81, 739-743, 1973.

Hwang, P. A Wave kinematics and sediment suspension at wave breaking point, Ph.D. Dissertation, Dept. of Civil Engineering, University of Delaware, 1982.

Iversen, J. D., Greeley, R., White, B. R., and Pollack, J. B., The effect of vertical distortion in the modeling of sedimentation phenomena, *J. Geophys. Res.*, 81, 4846-4856, 1976.

Jaenicke, R., Properties of atmospheric aerosols, in *Numerical Data and Functional Relationships in Sci. & Tech. (Landolt-Bornstein)*, ed. G. Fischer, Springer-Verlag, Gr. V, v. 4, ch. 9, 1988.

Junge, C. E., Our knowledge of the physico-chemistry of aerosols in the undisturbed marine environment, *J. Geophys. Res.*, 77, 5183-5200, 1972.

Kawamura, R., Study on sand movement by wind, Inst. of Science and Technology, Rep. 5, 95-112, 1951.

Kerr, D. E., *Propagation of Short Radio Waves*, McGraw-Hill Book Co., 1951 (reprinted by Peninsula Publishing, 1988).

Lettau, K. and Lettau, H., Experimental and micro-meteorological field studies of dune migration, in Exploring the world's driest climate, U. Wisconsin-Madison, Inst. Envir. Studies, IES Rep. 101, 110-147, 1978.

Mie, G. 1908. Contributions to the optics of suspended media, specifically colloidal metal suspensions, *Annelen d. Physik*, 25, 377-455.

Nickling, W. G., Eolian sediment transport, Slims River Valley, Yukon Territory, Ph.D. Dissertation, Dept. Geography and Regional Planning, U. Ottawa, 1975.

Nickling, W. G., Eolian sediment transport during dust storms: Slims River Valley, Yukon Territory, *Can. J. Earth Sci.*, 15, 1069-1084, 1978.

Nickling, W. G., Grain-size characteristics of sediment transported during dust storms, *J. Sed. Pet.*, 53, 1011-1024, 1983.

Owen, P. R., Saltation of uniform grains in air, *J. Fluid Mech.*, 20, 225-242, 1964.

Raudkivi, A. J., A. J. *Loose Boundary Hydraulics*, 2nd ed., Pergamon Press, New York, 1976.

Rayleigh, J. W. S., *The Theory of Sound, Vol. I & II*, Dover, 1945.

Sarre, R. D., Aeolian sand transport, *Prog. Phys. Geogr.*, 11, 157-182, 1987.

Schlichting, H., *Boundary-Layer Theory*, McGraw-Hill, 1968.

Schmidt, R. A., Properties of blowing snow, *Rev. Geophys. and Space Phys.*, 20, 39-44, 1982.

Sleath, J. F. A., *Sea Bed Mechanics*, Wiley Interscience, New York, 1984.

Sommerfeld, A., *Optics. Lectures on Theoretical Physics Vol IV.* Academic Press, 1950.

Stutzman, W. L., and Thiele, G. A., *Antenna Theory and Design*, John Wiley & Sons, 1981.

Toba, Y., On the giant sea-salt particles in the atmosphere. 1. General features of the distribution, *Tellus*, 1, 131-145, 1965.

Ungar, J. E., and P. K. Haff, Steady state saltation in air, *Sedimentology*, 34, 289-299, 1987.

van de Hulst, H. C., *Light scattering by small particles*, Dover Publications, New York, 1981.

Werner, B. T., A physical model of wind-blown sand transport, Ph.D. Dissertation, California Institute of Technology, 1987.

Werner, B. T., A steady-state model of wind-blown sand transport, *J. Geol.*, 98, 1-17, 1990.

White, B. R., Soil transport on Mars, *J. Geophys. Res.*, 84,4643-3651, 1979.

White, B. R. and J. C. Schulz, Magnus effect in saltation, *J. Fluid Mech*, 81, 497-512, 1977.

Willets, B. B., Transportation by wind of granular materials of different grain shapes and densities, *Sedimentology*, 30, 669-679, 1983.

Willets, B. B., M. A. Rice and S. E. Swaine, Shape effects in aeolian grain transport, *Sedimentology*, 29, 409-417, 1982.

Williams, G. Some aspects of the eolian saltation load, *Sed.*, 3, 257-287, 1964.

Yalin, M. S., *Mechanics of Sediment Transport*, 2nd ed., Pergamon Press, 1977.

Zingg, A. W., A study of the characteristics of sand movement by wind, Master's thesis, Dept. Agricultural Eng., Kansas State College of Agriculture and Applied Science, 1952.